



This discussion paper is/has been under review for the journal Atmospheric Measurement Techniques (AMT). Please refer to the corresponding final paper in AMT if available.

# Strato-mesospheric CIO observations by SMILES: error analysis and diurnal variation

T. O. Sato<sup>1,2</sup>, H. Sagawa<sup>1</sup>, D. Kreyling<sup>1</sup>, T. Manabe<sup>3</sup>, S. Ochiai<sup>1</sup>, K. Kikuchi<sup>1</sup>,  
P. Baron<sup>1</sup>, J. Mendrok<sup>4</sup>, J. Urban<sup>5</sup>, D. Murtagh<sup>5</sup>, M. Yasui<sup>1</sup>, and Y. Kasai<sup>1,2</sup>

<sup>1</sup>National Institute of Information and Communications Technology, 4-2-1 Nukui-kitamachi, Koganei, Tokyo, 184-8795, Japan

<sup>2</sup>Tokyo Institute of Technology, 4259 Nagatsuta-cho, Midori-ku, Yokohama, Kanagawa, 226-8503, Japan

<sup>3</sup>Osaka Prefecture University, 1-1 Gakuen-cho, Naka, Sakai, Osaka, 599-8531, Japan

<sup>4</sup>Luleå University of Technology, P.O. Box 812, 98128 Kiruna, Sweden

<sup>5</sup>Chalmers University of Technology, 41296 Gothenburg, Sweden

Received: 24 May 2012 – Accepted: 14 June 2012 – Published: 4 July 2012

Correspondence to: T. O. Sato (sato.t.ak@m.titech.ac.jp)

Published by Copernicus Publications on behalf of the European Geosciences Union.

Title Page

Abstract

Introduction

Conclusions

References

Tables

Figures

◀

▶

◀

▶

Back

Close

Full Screen / Esc

Printer-friendly Version

Interactive Discussion



## Abstract

Chlorine monoxide (ClO) is the key species for anthropogenic ozone loss in the middle atmosphere. We observed the ClO diurnal variation using the Superconducting Submillimeter-Wave Limb-Emission Sounder (SMILES) on the International Space Station which has a non sun-synchronous orbit. This is the first global observation of the ClO diurnal variation from the stratosphere up to the mesosphere. The SMILES observation reproduced the diurnal variation of stratospheric ClO, an enhancement during a daytime, as observed by the Microwave Limb Sounder on the Upper Atmosphere Research Satellite (UARS/MLS). Mesospheric ClO has shown a different diurnal behavior with an enhancement during nighttime. The ClO enhancement was found at a pressure of 0.02 hPa (about 70 km) with an amplitude of about 100 pptv and reached up to 0.01 hPa (80 km) in the zonal mean of 50° N–65° N in January–February 2010. The observation of mesospheric ClO was possible due to the 10–20 times better signal-to-noise ratio of the spectra than those of past microwave/submillimeter-wave limb-emission sounders. We performed a quantitative error analysis for the strato- and mesospheric ClO of the Level-2 research (L2r) product version 2.1.5 taking into account all possible error contributions; i.e. errors due to spectrum noise, smoothing and uncertainties in the radiative transfer model and instrument function. The SMILES L2r v2.1.5 ClO data are useful over the range 0.01 and 100 hPa with a total error of 10–30 pptv (about 10 %) with averaging of 100 profiles. The vertical resolution is 3–5 km and 5–8 km for the stratosphere and mesosphere, respectively. The performance of the SMILES observation opens the new opportunity to investigate ClO up to the mesopause.

## 1 Introduction

Chlorine monoxide (ClO) is the primary form of reactive chlorine and a key intermediate for ozone loss. The partitioning of the reactive form and reservoir form of the halogen

AMTD

5, 4667–4710, 2012

## Error analysis and diurnal variation of SMILES ClO observation

T. O. Sato et al.

[Title Page](#)

[Abstract](#)

[Introduction](#)

[Conclusions](#)

[References](#)

[Tables](#)

[Figures](#)

◀

▶

◀

▶

[Back](#)

[Close](#)

[Full Screen / Esc](#)

[Printer-friendly Version](#)

[Interactive Discussion](#)



species modulates ozone destruction. Chemical ozone loss is mostly controlled by the spatio-temporal distribution of active halogens. For example, ClO activation due to low temperatures produced the Arctic ozone hole in winter 2011 (Manney et al., 2011). Microwave spectroscopic remote sensing from space is one of the best methods to obtain the global ClO distribution in the Earth's middle atmosphere. There are four instruments on satellites so far to observe the ClO global distribution. The first satellite observation of ClO was performed by the Microwave Limb Sounder (MLS) on board the Upper Atmosphere Research Satellite (UARS), which was launched by NASA in 1991 (Waters et al., 1993); the UARS/MLS had observed the ClO transition at 204.4 GHz. The Sub-millimetre Radiometer on board the Odin satellite (Odin/SMR) was launched in February 2001 and observes ClO using the transition at 501.3 GHz (Murtagh et al., 2002). Aura/MLS was launched in 2004 and observes ClO using the transition at 649.4 GHz (Waters et al., 2006). The Superconducting Submillimeter-Wave Limb-Emission Sounder (SMILES) also observed ClO using the same transition as Aura/MLS but with much more sensitive technology. SMILES made observations from the Japanese Experiment Module (JEM) of the International Space Station (ISS) between 12 October 2009 and 21 April 2010 (Kikuchi et al., 2010).

The SMILES observations are notable in that they are (1) the first passive observations of the Earth's atmosphere with a sensitive 4-K submillimeter-wave receiver and (2) a sensitive observations of short-lived atmospheric compositions with diurnal variation, which is achieved by the non sun-synchronous orbit of the ISS.

The SMILES instrument employs superconductor-insulator-superconductor (SIS) mixers cooled at about 4 K and high-electron-mobility-transistor (HEMT) amplifiers at 20 and 100 K. The receiver system achieves a quite low system noise temperature ( $T_{\text{sys}}$ ) of about 350 K and a signal-to-noise (S/N) ratio of about 50 for stratospheric ClO at mid-latitudes for a single-scan spectrum.  $T_{\text{sys}}$  achieved with receiver systems using a conventional Schottky diodes is about 3000–6000 K in the 500–600 GHz region for passive satellite observations using a submillimeter-wave. SMILES observes the atmospheric compositions of major and minor species using the low noise receiver

## Error analysis and diurnal variation of SMILES ClO observation

T. O. Sato et al.

[Title Page](#)

[Abstract](#)

[Introduction](#)

[Conclusions](#)

[References](#)

[Tables](#)

[Figures](#)

[◀](#)

[▶](#)

[Back](#)

[Close](#)

[Full Screen / Esc](#)

[Printer-friendly Version](#)

[Interactive Discussion](#)

system. The target species of SMILES are O<sub>3</sub>, ClO, H<sup>35</sup>Cl, H<sup>37</sup>Cl, O<sub>3</sub> isotopomers, BrO, HO<sub>2</sub>, HOCl, CH<sub>3</sub>CN and HNO<sub>3</sub> in the stratosphere and mesosphere, as well as H<sub>2</sub>O and ice clouds in the upper troposphere/lower stratosphere. SMILES has three observation frequency bands: band A (624.32–625.52 GHz), band B (625.12–626.32 GHz) and band C (649.12–650.32 GHz). The ClO transitions observed by SMILES in the ground ro-vibronic state ( $\Lambda$ -type doubling,  $J = 35/2-33/2$ ) are located at 649.445 and 649.451 GHz in band C (Fig. 1). Two of the three frequency bands were used simultaneously, as in simultaneous observations using bands A and B, bands B and C, bands C and A, since SMILES has two spectrometers. About 70 % of all observations were performed for band C. The SMILES instrument observed the Earth's limb from the JEM/ISS at an altitude of 330–370 km. The latitudes covered by SMILES observations were normally 38° S–65° N. About 1600 points were observed per day by SMILES. The tangent height region of antenna scanning was nominally 0–100 km.

We quantitatively evaluated the total error of the ClO observation taking into account all known error contributions; i.e. errors due to spectrum noise, smoothing, uncertainties in the radiative transfer model and instrument function. The error due to inaccuracy in the spectrum calibration was also evaluated. The uncertainties were conservatively determined based on the laboratory and in-orbit measurements made by the SMILES mission team, for the Level-2 research (L2r) product version 2.1.5. Section 2 describes all error sources considered in this sturdy and calculation methods of the errors for the SMILES ClO observation. Section 3 describes the results and discussions of the error analysis. Section 4 describes the diurnal variations observed by SMILES. The stratospheric ClO diurnal variations observed by SMILES and UARS/MLS are compared. We observed the global diurnal variation of mesospheric ClO for the first time.

## 25 2 Method of error characterization

We performed an error analysis for the retrieval ClO VMR profile using a single-scan spectrum. The error on the ClO profile comes from spectrum statistics noise and

## Error analysis and diurnal variation of SMILES ClO observation

T. O. Sato et al.

[Title Page](#)

[Abstract](#)

[Introduction](#)

[Conclusions](#)

[References](#)

[Tables](#)

[Figures](#)

[◀](#)

[▶](#)

[Back](#)

[Close](#)

[Full Screen / Esc](#)

[Printer-friendly Version](#)

[Interactive Discussion](#)

uncertainty and inaccuracy in the spectrum synthesis using forward model and spectrum calibration.

## 2.1 Uncertainties in the synthesized and observed spectra

### 2.1.1 Radiative transfer calculation

5 We used the Advanced Model for Atmospheric Tera Hertz Radiation Analysis and Simulation (AMATERASU) (Baron et al., 2008) for the clear-sky radiative transfer calculation and instrument function, which is also used for the calculation of L2r version 2.1.5 (Baron et al., 2011). The details of the forward model calculation are described in Urban et al. (2004). The intensity of radiance at the frequency  $\nu$  is calculated using the  
10 total absorption coefficient  $k_\nu$ .

$$k_\nu(s) = \sum_{p,q} \rho^p(s) J_{\nu_q}^q(T) \frac{\nu}{\nu_q} f_\nu(\nu_q, w_q) + k_\nu^{\text{cont}}(s), \quad (1)$$

15 where  $s$  is the line-of-sight,  $\rho^p(s)$  is the number density of species  $p$ ,  $\nu_q$  is the frequency of transition  $q$ ,  $J_{\nu_q}^q(T)$  is the line intensity of transition  $q$  at temperature  $T$ ,  $f_\nu(\nu_q, w_q)$  is the line shape function for transition  $q$ ,  $w_q$  is the line width of transition  $q$  and  $k_\nu^{\text{cont}}(s)$  is the continuum absorption coefficient. The line width  $w$  consists of the collisional broadening width  $w_{\text{col}}$  and the Doppler broadening width  $w_{\text{dop}}$ .  $w_{\text{col}}$  is described using the air-broadening coefficient  $\gamma_{\text{air}}$  as

$$w_{\text{col}} = \gamma_{\text{air}}(T)P(1 - x_{\text{VMR}}) + \gamma_{\text{self}}(T)P x_{\text{VMR}}, \quad (2)$$

20 where  $P$  is pressure,  $x_{\text{VMR}}$  is the volume mixing ratio (VMR) and  $\gamma_{\text{self}}$  is the self-broadening coefficient. The contribution of the self-broadening is smaller than that of air-broadening since  $x_{\text{VMR}}$  of the interest species is small (in case of CIO, the order of VMR is less than  $10^{-9}$ ).  $\gamma_{\text{air}}$  depends on temperature  $T$  with a factor  $n_{\text{air}}$  written as

Title Page

Abstract

Introduction

Conclusions

References

Tables

Figures

◀

▶

◀

▶

Back

Close

Full Screen / Esc

Printer-friendly Version

Interactive Discussion

$$\gamma_{\text{air}}(T) = \gamma_{\text{air}}(T_0) \left( \frac{T}{T_0} \right)^{-n_{\text{air}}} \quad (T_0 = 296\text{K}) . \quad (3)$$

The line-by-line calculation was performed using the dedicated spectroscopic database for SMILES observations. The lines included in the SMILES spectroscopic database were selected according to the line selection algorithm (Sato, 2010; Baron et al., 2011) from the lines listed in the JPL spectroscopic catalog (Pickett et al., 1998) and HITRAN 2008 catalog (Rothman et al., 2009). The number of lines in the SMILES spectroscopic database was about 1200. The line intensities and transition frequencies were adopted from the JPL catalog with some replacements with recent laboratory measurements (Cazzoli and Puzzarini, 2004, H. Ozeki, personal communication, 2010; W. G. Read, personal communication, 2011). The air-broadening coefficients,  $\gamma_{\text{air}}$  and  $n_{\text{air}}$ , were taken from the HITRAN 2008 catalog (Rothman et al., 2009) and the laboratory measurements such as (Drouin and Gamache, 2008; Hoshina et al., 2008; Sato et al., 2010; Drouin, 2007; Markov and Krupnov, 1995; Mizoguchi et al., 2012; Perrin et al., 2005, W. G. Read, personal communication, 2011). The spectroscopic parameters and their references of the CIO lines observed by SMILES are given in Table 1. A Van Vleck and Weisskopf profile (van Vleck and Weisskopf, 1945) was used as a line shape function at lower altitudes where the Doppler broadening width was less than 1/40th of the collisional broadening width, and a Voigt profile (Schreier and Kohlert, 2008) was used at higher altitudes. The continuum absorption coefficients of the humidity and dry-air employed were based on atmospheric opacity measurements made by Pardo et al. (2001). The dry-air continuum model was multiplied by 1.2 to be more consistent with theoretical estimation; e.g. (Boissoles et al., 2003).

We estimated the errors for the CIO VMR retrievals due to uncertainties in line intensity,  $\gamma_{\text{air}}$  and  $n_{\text{air}}$  of the CIO lines. The typical uncertainties given in Table 1 were used in this error analysis; i.e. 1 %, 3 % and 10 % for line intensity (Pickett et al., 1998),  $\gamma_{\text{air}}$  and  $n_{\text{air}}$  (Oh and Cohen, 1994, W. G. Read, personal communication, 2011), respectively. As a representative of the effect of other molecular transitions, the effect

## Error analysis and diurnal variation of SMILES CIO observation

T. O. Sato et al.

[Title Page](#)

[Abstract](#)

[Introduction](#)

[Conclusions](#)

[References](#)

[Tables](#)

[Figures](#)

◀

▶

[Back](#)

[Close](#)

[Full Screen / Esc](#)

[Printer-friendly Version](#)

[Interactive Discussion](#)

## Error analysis and diurnal variation of SMILES CIO observation

T. O. Sato et al.

[Title Page](#)

[Abstract](#)

[Introduction](#)

[Conclusions](#)

[References](#)

[Tables](#)

[Figures](#)

[◀](#)

[▶](#)

[◀](#)

[▶](#)

[Back](#)

[Close](#)

[Full Screen / Esc](#)

[Printer-friendly Version](#)

[Interactive Discussion](#)



of  $\gamma_{\text{air}}$  of the strong O<sub>3</sub> line at 650.732 GHz was evaluated. The wing of this O<sub>3</sub> line contributes largely to the baseline of the band C spectrum. We adopted  $\gamma_{\text{air}}$  of O<sub>3</sub> of 3.01 MHz Torr<sup>-1</sup> measured by Drouin and Gamache (2008). The error in the CIO VMR due to 3 % uncertainty was estimated. We also estimated the error for the CIO retrieval due to 20 % uncertainty in the dry-air continuum model.

Temperature and pressure for the radiative transfer calculation were taken from the Goddard Earth Observing System Model, Version 5.2 (GEOS-5) (Rienecker et al., 2008) and the MSIS climatology (Hedin, 1991) for the altitude region from the surface to 70 km and that from 70 to 110 km, respectively. The uncertainties in the temperature profile have been conservatively estimated according to a comparison of temperatures measured from Aura/MLS and GEOS-5 (Schwartz et al., 2008); i.e. 3, 10, 30 and 50 K for the troposphere (below 11 km), the stratosphere (11–59 km), the mesosphere (59–96 km) and the thermosphere (above 96 km). The uncertainties in the pressure profile were conservatively set as constant percentages of 10 % for all altitudes.

### 2.1.2 Instrument function

#### Uncertainty in the instrumental part of the forward model

Here, we describe key instrument functions of SMILES such as the antenna beam pattern, the separation ratio of the sideband separator (SBS) and the filter response function of each channel in the spectrometer. Figure 2 shows the signal flow in the SMILES system. Further details of the SMILES instrument are described by Kikuchi et al. (2010); Masuko et al. (2002) and Ochiai et al. (2012b).

The optical path of SMILES is well designed to minimize standing waves (the spectral ripple is as small as 0.09 % of the input brightness temperature Ochiai et al., 2012b) so that their effects are negligible in this error analysis.

The aperture size of the offset-Cassegrain antenna (ANT) is 400 mm × 200 mm (Manabe et al., 2012). Its vertical beam size is 0.09°, in terms of the full width at half maximum (FWHM), and the field-of-view is around 3.2–4.4 km at tangent heights ranging

Title Page

Abstract

Introduction

Conclusions

References

Tables

Figures

◀

▶

◀

▶

Back

Close

Full Screen / Esc

Printer-friendly Version

Interactive Discussion

from 10 to 60 km. The radiance  $I_v^{\text{ANT}}$  at the frequency  $v$  received by a boresight solid angle of ANT is given by

$$I_v^{\text{ANT}} = \int_{\Omega_0} I_v(\Omega) R_v^{\text{ANT}}(\Omega) d\Omega, \quad (4)$$

where  $I_v(\Omega)$  is the radiance for the direction  $\Omega$ ,  $R_v^{\text{ANT}}$  is a normalized antenna beam pattern of ANT and  $\Omega_0$  is the boresight solid angle. The solid angle  $\Omega_0$  is defined in the Level-1 processing as the angular range within  $\pm 4.2^\circ$  from the boresight direction. The Level-1 brightness temperature does not include the radiance coming from outside of  $\Omega_0$ , which is estimated and subtracted from the total radiance in the Level-1 process. The error due to emission from outside of  $\Omega_0$  is described later. The SMILES instrument periodically scans the atmosphere with a stepping rate of 12 Hz and an angular step of  $0.009375^\circ$ . The atmospheric limb emissions during six steps in 0.5 s are accumulated to generate a spectrum at one tangent height. The forward model in the L2r v2.1.5 synthesizes a spectrum at one tangent height using  $R_v^{\text{ANT}}$  without adjustments for the antenna movement over six scan steps. The errors in the CIO retrieval due to the omission of the adjustments and an uncertainty in the beam size were calculated. The beam-size uncertainty used in the error analysis was 2 %, which was conservatively estimated from the measurement error in the pre-launch test of antenna beam pattern.

The upper sideband (USB) and the lower sideband (LSB) are separated using SBS and fed to the SIS mixers for USB and LSB, respectively. The configuration of SBS is described in (Manabe et al., 2003). The radiance input to the USB mixer ( $I_{v_{\text{IF}}}^{\text{UMIX}}$ ) can be expressed using the radiances in the USB ( $I_{v_{\text{USB}}}^{\text{ANT}}$ ) and LSB ( $I_{v_{\text{LSB}}}^{\text{ANT}}$ ) received by ANT as follows.

$$I_{v_{\text{IF}}}^{\text{UMIX}} = \beta_{v_{\text{IF}}}^{\text{USB}} I_{v_{\text{USB}}}^{\text{ANT}} + (1 - \beta_{v_{\text{IF}}}^{\text{USB}}) I_{v_{\text{LSB}}}^{\text{ANT}}, \quad (5)$$

$$v_{\text{IF}} = v_{\text{USB}} - v_{\text{LO}} = v_{\text{LO}} - v_{\text{LSB}}, \quad (6)$$

## Error analysis and diurnal variation of SMILES CIO observation

T. O. Sato et al.

[Title Page](#)

[Abstract](#)

[Introduction](#)

[Conclusions](#)

[References](#)

[Tables](#)

[Figures](#)

[◀](#)

[▶](#)

[◀](#)

[▶](#)

[Back](#)

[Close](#)

[Full Screen / Esc](#)

[Printer-friendly Version](#)

[Interactive Discussion](#)

where  $\beta_{\nu_{\text{IF}}}^{\text{USB}}$  is the contribution ratio of  $I_{\nu_{\text{USB}}}^{\text{ANT}}$  and  $\nu_{\text{LO}}$  is the frequency of the local oscillator at 637.32 GHz. Ochiai et al. (2008) describes the detail of  $\beta_{\nu_{\text{IF}}}^{\text{USB}}$ .  $\beta_{\nu_{\text{IF}}}^{\text{USB}}$  ranges between 0.98 and 0.99 but it is assumed to be one to reduce the calculation time in the retrieval processing of L2r v2.1.5. We calculated the errors in the CIO retrieval due to this assumption and the uncertainty in  $\beta_{\nu_{\text{IF}}}^{\text{USB}}$  of  $\pm 3\text{dB}$ .

Two acousto-optical spectrometers (AOSs), named UNIT 1 and UNIT 2, are used for the SMILES spectral detection. The response functions of the AOS were measured in orbit (Mizobuchi et al., 2012). The UNIT 1 of the AOS is used for CIO observations. The CIO transitions at 649.445 and 649.451 GHz typically locate at the AOS channels around 535. The full width at half maximum (FWHM) of the response function is about 1.06 MHz at channel 535 of the UNIT 1. The uncertainty in the FWHM was conservatively estimated as 10 %.

### Calibration uncertainty

Level-1b (L1b) version 007 data are used for processing of L2r v2.1.5. We give a brief overview of the calibration procedure in L1b version 007. Hereafter we represent the radiance / by brightness temperature  $\mathcal{T}$ .

The brightness temperature averaged over  $\Omega_0$  with a weight of  $R^{\text{ANT}}$  is denoted as  $\mathcal{T}_{\text{ANT}}$ . The total brightness temperature  $\mathcal{T}_{\text{MR}}$  received by ANT at the point of the main reflector (MR) is expressed as

$$20 \quad \mathcal{T}_{\text{MR}} = \eta_{\text{main}} \mathcal{T}_{\text{ANT}} + \eta_{\text{space}} \mathcal{T}_{\text{B}}(T_{\text{space}}) + \eta_{\text{earth}} \mathcal{T}_{\text{B}}(T_{\text{earth}}) + \eta_{\text{body}} \mathcal{T}_{\text{B}}(T_{\text{body}}), \quad (7)$$

where  $\eta_{\text{main}}$  is the main beam efficiency in the solid angle region defined by  $\Omega_0$ .  $\eta_{\text{space}}$ ,  $\eta_{\text{earth}}$  and  $\eta_{\text{body}}$  are the fractions of antenna beam pattern integrated over the solid angles which direct toward the space, the Earth and the SMILES structural body, respectively,  $T_{\text{space}}$ ,  $T_{\text{earth}}$  and  $T_{\text{body}}$  are the temperatures of the space, the Earth and the SMILES structural body, respectively.  $\mathcal{T}_{\text{B}}(T)$  represents the brightness temperature of

a black body at temperature  $T$ . The main beam efficiency  $\eta_{\text{main}}$  is 0.975 in L1b version 007. We conservatively estimated the uncertainty in  $\eta_{\text{main}}$  as 2%.

The fractional contributions of the space, the Earth and the SMILES structural body ( $\eta_{\text{space}}$ ,  $\eta_{\text{earth}}$  and  $\eta_{\text{body}}$ , respectively) are geometrically calculated as

5  $\eta_{\text{space}} = 0.084(1 - \eta_{\text{main}})$ ,  
 $\eta_{\text{earth}} = 0.060(1 - \eta_{\text{main}})$ ,  
 $\eta_{\text{body}} = 0.856(1 - \eta_{\text{main}})$ , (8)

for limb observation, and

10  $\eta_{\text{space}} = 0.140(1 - \eta_{\text{main}})$ ,  
 $\eta_{\text{earth}} = 0.004(1 - \eta_{\text{main}})$ ,  
 $\eta_{\text{body}} = 0.856(1 - \eta_{\text{main}})$ , (9)

15 for the cold-reference measurement (cosmic microwave background). In the L1b version 007 process, we assume that  $\mathcal{T}_B(T_{\text{space}})$  is substantially 0 K,  $T_{\text{earth}}$  is 255 K, and  $T_{\text{body}}$  is the measured physical temperature of the antenna structure.  $T_{\text{earth}}$  has the largest variation among  $T_{\text{space}}$ ,  $T_{\text{earth}}$  and  $T_{\text{body}}$ . We investigated the errors due to uncertainties in  $T_{\text{earth}}$  of 20 K, which is a typical variation in the actual Earth's atmosphere.

20 The Joule losses of mirrors are taken into account. The brightness temperature due to losses of the main reflector (MR), sub reflector (SR) and tertiary reflector (TR) are not calibrated by comparison with the reference brightness temperature from the calibration hot load (CHL), which is measured every 53 s by inserting a switch mirror (SWM) in the beam between the tertiary and fourth mirrors. The brightness temperature  $\mathcal{T}_{\text{TR}}^{\text{atm}}$  of the beam between the tertiary and fourth mirrors at atmospheric measurement is expressed as

25 
$$\mathcal{T}_{\text{TR}}^{\text{atm}} = \mu_{\text{MR}}\mu_{\text{SR}}\mu_{\text{TR}}\mathcal{T}_{\text{MR}} + (1 - \mu_{\text{MR}}\mu_{\text{SR}}\mu_{\text{TR}})\mathcal{T}_B(T_{\text{mirror}}), \quad (10)$$

[Title Page](#)

[Abstract](#)

[Introduction](#)

[Conclusions](#)

[References](#)

[Tables](#)

[Figures](#)

[◀](#)

[▶](#)

[◀](#)

[▶](#)

[Back](#)

[Close](#)

[Full Screen / Esc](#)

[Printer-friendly Version](#)

[Interactive Discussion](#)



## Error analysis and diurnal variation of SMILES CIO observation

T. O. Sato et al.

[Title Page](#)

[Abstract](#) [Introduction](#)

[Conclusions](#) [References](#)

[Tables](#) [Figures](#)

◀

▶

◀

▶

[Back](#) [Close](#)

[Full Screen / Esc](#)

[Printer-friendly Version](#)

[Interactive Discussion](#)

where  $\mu_{\text{MR}}$ ,  $\mu_{\text{SR}}$  and  $\mu_{\text{TR}}$  are transmission coefficients of MR, SR and TR, respectively, and  $T_{\text{mirror}}$  is the temperature of the reflectors. These three reflectors are assumed to have the same temperature  $T_{\text{mirror}}$ . The scattering and spillover losses at these reflectors are counted in the efficiency  $\eta_{\text{body}}$  and not in  $\mu_{\text{MR}}$ ,  $\mu_{\text{SR}}$  and  $\mu_{\text{TM}}$ . The brightness temperature  $\mathcal{T}_{\text{TR}}^{\text{hot}}$  of the beam for the hot-reference brightness temperature at TR is

$$\mathcal{T}_{\text{TR}}^{\text{hot}} = \mu_{\text{SWM}} \{ \mu_{\text{CHL}} \mathcal{T}_{\text{B}}(T_{\text{CHL}}) + (1 - \mu_{\text{CHL}}) \mathcal{T}_{\text{RX}} \} + (1 - \mu_{\text{SWM}}) \mathcal{T}_{\text{B}}(T_{\text{mirror}}), \quad (11)$$

where  $\mu_{\text{SWM}}$  is transmission coefficients of SWM,  $\mu_{\text{CHL}}$  is one minus the return loss of CHL,  $T_{\text{CHL}}$  is the temperature of CHL and  $\mathcal{T}_{\text{RX}}$  is the brightness temperature coming from CHL to the receiver. The coefficients  $\mu_{\text{MR}}$ ,  $\mu_{\text{SR}}$ ,  $\mu_{\text{TR}}$  and  $\mu_{\text{SWM}}$  are 0.9955, 0.9958, 0.9956 and 0.9959, respectively, which are estimated from reflection measurements in laboratory of materials that have the identical surfaces with the reflectors. The uncertainties in these coefficients were estimated to be 0.1 %. The power reflection coefficient of CHL is negligibly small (less than  $-60\text{dB}$ ) and  $\mu_{\text{CHL}}$  is assumed to be one.

The receiver output, i.e. the quantized output from the AOS, is deviated from a linear relation to the input brightness temperature because of gain nonlinearity of the receiver and spectrometer components. The output  $V_{\nu}$  from the AOS at the channel corresponding to the frequency  $\nu$  is given by

$$V_{\nu} = G_{\nu} (1 - \alpha \bar{V} - \alpha' V_{\nu}) p_{\nu} + V_0, \quad (12)$$

where  $G_{\nu}$  is the total system gain,  $\bar{V}$  is an average of  $V_{\nu}$  over the whole spectrometer channels,  $V_0$  is the offset of the AOS output and  $p_{\nu}$  is the total input power to the receiver.  $\bar{V}$  is assumed to be 12 000 and 22 500 for the cold reference in this error analysis. The input power  $p_{\nu}$  is proportional to the sum of  $\mathcal{T}_{\text{ANT}}$  and the system noise temperature  $\mathcal{T}_{\text{sys}}$ ;  $\mathcal{T}_{\text{sys}}$  includes system noise, the brightness coming into the direction  $\Omega_0$  and emissions from lossy reflectors. The coefficients  $\alpha$  and  $\alpha'$  represent the receiver gain nonlinearity (Ochiai et al., 2012a).  $\alpha$  is  $1.884 \times 10^{-6}$  and is measured in the pre-launch test. We call  $\alpha$  the “gain-compression parameter”. We conservatively estimated

the uncertainty in  $\alpha$  as 20 %. The term  $\alpha'V_\nu$  does not have large effects on the CIO retrieval comparing with the term  $\alpha\bar{V}$  and was ignored in this error analysis.

The Level-1 processing produces the brightness temperature spectrum  $\mathbf{y}_{\text{obs}}$ , which is the estimation of  $\mathcal{T}_{\text{ANT}}$  using  $V_\nu$  for atmospheric limb-observation, the cold reference (space) and the hot (CHL) references (Ochiai et al., 2008).

## 2.2 Inversion analysis

We employed the Optimal Estimation Method (Rodgers, 2000) for the retrieval analysis in L2r version 2.1.5 (Baron et al., 2011). The method leads to the maximum a posteriori solution, which minimizes the value of  $\chi^2$ :

$$10 \quad \chi^2 = [\mathbf{y}_{\text{obs}} - \mathcal{F}(\mathbf{x}, \mathbf{b})]^T \mathbf{S}_y^{-1} [\mathbf{y}_{\text{obs}} - \mathcal{F}(\mathbf{x}, \mathbf{b})] + (\mathbf{x} - \mathbf{x}_a)^T \mathbf{S}_a^{-1} (\mathbf{x} - \mathbf{x}_a), \quad (13)$$

where  $\mathcal{F}$  is the forward model,  $\mathbf{x}$  is a vector of the atmospheric true state,  $\mathbf{b}$  is a vector of the parameters used in  $\mathcal{F}$ ,  $\mathbf{S}_y$  is the covariance matrix for the spectrum noise  $\epsilon_y$ ,  $\mathbf{x}_a$  is an a priori state of  $\mathbf{x}$  and  $\mathbf{S}_a$  is the covariance matrix for the natural variability of  $\mathbf{x}$ . We use  $\mathbf{S}_y$  and  $\mathbf{S}_a$  as tuning parameters to obtain a stable result of the retrieval analysis.

$$15 \quad \mathbf{S}_y[i, j] = \epsilon_y^2 \delta_{i,j}, \quad \epsilon_y = 0.5 \text{K}, \quad (14)$$

where  $\delta_{i,j}$  is a Kronecker delta.

$$20 \quad \mathbf{S}_a[i, j] = \epsilon_a[i] \epsilon_a[j] \exp\left[-\frac{|z[i] - z[j]|}{z_c}\right], \quad (15)$$

$$\epsilon_a[i] = \epsilon_1 \mathbf{x}_a[i] + \epsilon_2, \quad (\epsilon_1, \epsilon_2) = (0.5, 2.0 \times 10^{-10}) \quad (16)$$

where  $z_c$  is a correlation length that constrains the vertical continuity in the retrieved profile, and is set to 6 km.

Title Page

Abstract

Introduction

Conclusions

References

Tables

Figures

◀

▶

◀

▶

Back

Close

Full Screen / Esc

Printer-friendly Version

Interactive Discussion

A vertical VMR profile of ClO is retrieved using each scan of the band C spectrum with a reduced frequency window of  $649.4 \pm 0.2$  GHz. We use the measurements whose tangent heights are in the range from 15 to 90 km. The accompanying retrieval parameters are a second-order polynomial baseline and an offset of the AOS frequency and a line-of-sight elevation angle for each scan. In addition, the VMR of  $\text{H}_2\text{O}$  is also set as variables with the intention of improving the fit of the baseline. Temperature and pressure profiles are not retrieved. The ClO a priori profile is the same as that for Odin/SMR, which is based on the UARS/MLS climatology. The weighting functions are calculated at altitudes from 16 to 43 km with 3-km intervals, from 43 to 55 km with 4-km intervals and from 55 to 95 km with 5-km intervals.

### 2.3 Error calculation method

The total error  $E_{\text{total}}$  is given by

$$E_{\text{total}}[i] = \sqrt{E_{\text{noise}}[i]^2 + E_{\text{smooth}}[i]^2 + E_{\text{param}}[i]^2 + E_{\text{calib}}[i]^2}, \quad (17)$$

where  $E_{\text{noise}}$  is the error due to spectrum noise,  $E_{\text{smooth}}$  is the smoothing error,  $E_{\text{param}}$  is the error due to uncertainty in the model parameter and  $E_{\text{calib}}$  is the error due to inaccuracy in the spectrum calibration. We conservatively estimated the uncertainties for each error source described in Sects. 2.1 and 2.2. We took the root-sum-square values for the estimation of total systematic error since we considered as many (16) error sources as possible and most of the error sources were conservatively estimated.

We assumed that the true state is identical to the a priori state  $\mathbf{x}_a$ , and synthesized the reference spectrum  $\mathbf{y}_{\text{ref}}$  using  $\mathbf{x}_a$ . The inversion calculation was performed using  $\mathbf{y}_{\text{ref}}$ . We used a retrieved state  $\mathbf{x}_{\text{ref}}$  (not  $\mathbf{x}_a$ ) as a reference profile for the error analysis and removed the characteristics included in the retrieval algorithm itself.

$$\mathbf{x}_{\text{ref}} = \mathcal{I}(\mathbf{y}_{\text{ref}}, \mathbf{b}_0), \quad (18)$$

where  $\mathcal{I}$  is the inversion function and  $\mathbf{b}_0$  is a vector of model parameters. The reference profile is shown in Fig. 3 with the difference in  $\mathbf{x}_a$  and  $\mathbf{x}_{\text{ref}}$ . This figure also shows the

Title Page

Abstract | Introduction

Conclusions | References

Tables | Figures

◀

▶

◀

▶

Back

Close

Full Screen / Esc

Printer-friendly Version

Interactive Discussion

measurement response  $\mathbf{m}$  and averaging kernel  $\mathbf{A}$ . The details of  $\mathbf{m}$  are explained by Baron et al. (2002) and we simplified as follows.

$$\mathbf{m}[i] = \sum_j |\mathbf{A}[i, j]| \quad (19)$$

$$\mathbf{A} = \frac{\partial \hat{\mathbf{x}}}{\partial \mathbf{x}} = \mathbf{D}\mathbf{K} \quad (20)$$

$$^5 \mathbf{D} = \frac{\partial \hat{\mathbf{x}}}{\partial \mathbf{y}} = \left( \mathbf{K}^T \mathbf{S}_y^{-1} \mathbf{K} + \mathbf{S}_a^{-1} \right)^{-1} \mathbf{K}^T \mathbf{S}_y^{-1} \quad (21)$$

$$\mathbf{K} = \frac{\partial \mathbf{y}}{\partial \mathbf{x}} \quad (22)$$

The weighting function  $\mathbf{K}$  is analytically calculated, and  $\mathbf{m}$ ,  $\mathbf{A}$  and contribution function  $\mathbf{D}$  are consecutively given using  $\mathbf{K}$  (Urban et al., 2004). The typical vertical resolutions of L2r version 2.1.5 is about 3–5 km and 5–8 km for the altitude region of 30–50 km and 50–70 km, respectively.

### 2.3.1 Retrieval error

The retrieval error consists of the error due to spectrum statistical noise  $E_{\text{noise}}$  and smoothing error  $E_{\text{smooth}}$ .

$$^5 \mathbf{S}_{\text{noise}} = \mathbf{D} \mathbf{S}_y \mathbf{D}^T, \\ E_{\text{noise}}[i] = \sqrt{\mathbf{S}_{\text{noise}}[i, i]}, \quad (23)$$

where  $\mathbf{S}_{\text{noise}}$  is the error covariance matrix for the measurement noise.

$$\mathbf{S}_{\text{smooth}} = (\mathbf{A} - \mathbf{U}) \mathbf{S}_a (\mathbf{A} - \mathbf{U})^T, \\ ^{20} E_{\text{smooth}}[i] = \sqrt{\mathbf{S}_{\text{smooth}}[i, i]}, \quad (24)$$

[Title Page](#)[Abstract](#)[Introduction](#)[Conclusions](#)[References](#)[Tables](#)[Figures](#)[◀](#)[▶](#)[Back](#)[Close](#)[Full Screen / Esc](#)[Printer-friendly Version](#)[Interactive Discussion](#)

where  $\mathbf{S}_{\text{smooth}}$  is the error covariance matrix for an error derived from  $\mathbf{S}_a$  and  $\mathbf{U}$  is the unit matrix. Note that  $\mathbf{E}_{\text{smooth}}$  has both aspects for being included in the random error ( $\mathbf{E}_{\text{random}}$ ) and systematic error ( $\mathbf{E}_{\text{systematic}}$ ). The random aspect in  $\mathbf{E}_{\text{smooth}}$  results from applying infinite vertical grids of the retrieved state  $\hat{\mathbf{x}}$  to true state  $\mathbf{x}$  and the systematic aspect is constraining  $\hat{\mathbf{x}}$  to  $\mathbf{x}_a$  where the measurement response  $\mathbf{m}$  is low. We focus on data of L2r version 2.1.5 that satisfies  $\mathbf{m} > 0.8$  in this paper. In this case,  $\mathbf{E}_{\text{smooth}}$  becomes more random than systematic. We categorize  $\mathbf{E}_{\text{smooth}}$  as  $\mathbf{E}_{\text{random}}$  in the following sturdy.

### 2.3.2 Uncertainty in model parameters

10 Errors due to uncertainties in the spectroscopic parameters, instrument functions and atmospheric profiles of temperature and pressure are categorized into  $\mathbf{E}_{\text{param}}$ .  $\mathbf{E}_{\text{param}}$  is calculated as

$$\mathbf{E}_{\text{param}} = \mathcal{J}(\mathbf{y}_{\text{ref}}, \mathbf{b}_0 + \Delta\mathbf{b}) - \mathcal{J}(\mathbf{y}_{\text{ref}}, \mathbf{b}_0), \quad (25)$$

where  $\mathbf{y}_{\text{ref}}$  is the reference spectra and  $\mathbf{b}_0$  a vector of model parameters.

15 For error calculations of the uncertainties in the atmospheric temperature and the pressure profile, we took into account the vertical correlation. We calculated the CIO errors due to the temperature and pressure profile employing singular value decomposition as follows. The model parameter  $\mathbf{b}_0$  has the correlated uncertainty  $\Delta\mathbf{b}$ .  $\mathbf{b}_0$  is represented with respect to the eigenfunctions of the covariance matrix  $\mathbf{S}_b$  to get a representation of  $\mathbf{b}_0$  with uncorrelated components, named  $\bar{\mathbf{b}}_0$  using an orthogonal matrix  $\mathbf{B}$  ( $\mathbf{B}\mathbf{B}^T = \mathbf{U}$ ).

$$\mathbf{b}_0 = \mathbf{B}\bar{\mathbf{b}}_0, \quad \bar{\mathbf{b}}_0 = \mathbf{B}^T\mathbf{b}_0. \quad (26)$$

20 The covariance matrix of  $\bar{\mathbf{b}}_0$  ( $\mathbf{S}_{\bar{b}}$ ) is a diagonal matrix and composed of the eigenvalues of  $\mathbf{S}_b$ .  $\mathbf{S}_{\bar{b}}$  is expressed using  $\mathbf{S}_b$  and  $\mathbf{B}$  as

$$\mathbf{S}_{\bar{b}} = \mathbf{B}^T\mathbf{S}_b\mathbf{B} \quad (27)$$

## Error analysis and diurnal variation of SMILES CIO observation

T. O. Sato et al.

[Title Page](#)

[Abstract](#)

[Introduction](#)

[Conclusions](#)

[References](#)

[Tables](#)

[Figures](#)

◀

▶

◀

▶

[Back](#)

[Close](#)

[Full Screen / Esc](#)

[Printer-friendly Version](#)

[Interactive Discussion](#)



The covariance matrix of the temperature uncertainties is expressed as

$$\mathbf{S}_b[i, j] = \epsilon_T[i] \epsilon_T[j] \exp \left\{ -\frac{(z[i] - z[j])^2}{2z_c^2} \right\}, \quad (28)$$

where  $\epsilon_T[i]$  is the temperature uncertainty at the  $i$ th altitude  $z[i]$  and  $z_c$  is the correlation height of 6 km.  $\mathbf{S}_b$  and  $\mathbf{B}$  are computed from  $\mathbf{S}_b$  using numerical linear algebra

5 packages. The CIO VMR error  $\epsilon_{\text{param}}^i$  due to the uncertainty at  $i$ th altitude level is given by

$$\epsilon_{\text{param}}^i = \mathcal{J} \left( \mathbf{y}_{\text{ref}}, \mathbf{b}_0 + \sqrt{\mathbf{S}_b[i, i]} \mathbf{B}^i \right) - \mathcal{J}(\mathbf{y}_{\text{ref}}, \mathbf{b}_0), \quad (29)$$

where  $\mathbf{B}^i$  is the  $i$ -th row vector of  $\mathbf{B}$ . All  $\epsilon_{\text{param}}^i$  values are added by taking the root-sum-square;

$$10 \quad \epsilon_{\text{param}}[i] = \sqrt{\sum_j \epsilon_{\text{param}}^j[i]^2}. \quad (30)$$

### 2.3.3 Calibration inaccuracy

Errors due to inaccuracies in the spectrum calibration  $E_{\text{calib}}$  are calculated as

$$E_{\text{calib}} = \mathbf{D} \Delta \mathbf{y}, \quad (31)$$

where  $\Delta \mathbf{y}$  is the brightness temperature difference given with the value of the calibration 15 parameter used in the L1b processing and the value with the uncertainty.

## 3 Results of error analysis

The error analysis was performed for all possible error sources listed in Table 2. We separately discuss the results of the error analysis for random error  $E_{\text{random}}$  and systematic error  $E_{\text{systematic}}$ .  $E_{\text{random}}$  can be decreased by averaging several profiles; on the

Title Page

Abstract

Introduction

Conclusions

References

Tables

Figures

◀

▶

◀

▶

Back

Close

Full Screen / Esc

Printer-friendly Version

Interactive Discussion

other hand,  $E_{\text{systematic}}$  is independent of the time and location of the measurement and remains constant.  $E_{\text{random}}$  consists of  $E_{\text{noise}}$ ,  $E_{\text{smooth}}$  and  $E_{\text{param}}$  due to temperature and pressure profiles.  $E_{\text{systematic}}$  consists of  $E_{\text{param}}$  due to uncertainties in spectroscopic parameters and SMILES instrument functions and  $E_{\text{calib}}$ . A total error for averaging  $N$  profiles is given by

$$E_{\text{total}}(N)[i] = \sqrt{E_{\text{systematic}}[i]^2 + \frac{E_{\text{random}}(1)[i]^2}{N}}, \quad (32)$$

where  $E_{\text{random}}(1)$  is the random error for a single scan observation.

### 3.1 Random error

Figure 4 shows the error budgets for  $E_{\text{random}}$ ; i.e.  $E_{\text{noise}}$ ,  $E_{\text{smooth}}$  and  $E_{\text{param}}$  for the temperature and pressure profiles. In this paper, we show both the absolute VMR error (left) and the relative error (right) for all results of the error calculation. The relative error is calculated as the absolute VMR error divided by  $x_{\text{ref}}$ .  $E_{\text{noise}}$  and  $E_{\text{smooth}}$  are less than 20 % at pressures between 0.6 and 20 hPa where the CIO VMR enhances. The errors in the CIO retrieval due to uncertainties in the atmospheric temperature and pressure profiles were calculated employing singular value decomposition (Eq. 30). The errors due to the temperature profile are within 5 % at pressures between 0.2 and 20 hPa and increase at pressures higher than 10 hPa, even though the smaller uncertainties are at those lower altitudes. The errors due to the pressure profile increase to more than 50 % at pressures higher than 2 hPa, and are almost constant as 10 %–20 % at pressures lower than 2 hPa. The temperature and pressure profiles are related with several other parameters such as  $\gamma_{\text{air}}$  and  $n_{\text{air}}$ , which makes larger the contribution of uncertainties in temperature and pressure profiles to the CIO retrieval.

The total random error is given by the root-sum-square of retrieval errors and errors due to temperature and pressure profiles. At pressures lower than 0.1 hPa, the retrieval errors are dominant and  $E_{\text{random}}$  increases from 50 to 200 pptv (>100%).  $E_{\text{random}}$  is

[Title Page](#)[Abstract](#)[Introduction](#)[Conclusions](#)[References](#)[Tables](#)[Figures](#)[◀](#)[▶](#)[◀](#)[▶](#)[Back](#)[Close](#)[Full Screen / Esc](#)[Printer-friendly Version](#)[Interactive Discussion](#)

about 30–50 pptv at pressures higher than 0.1 hPa. The pressure profile makes the largest contribution to the random error in the stratosphere.

## 3.2 Systematic error

### 3.2.1 Error due to uncertainty in spectroscopic parameters

Figure 5 shows the error budgets for the spectroscopic parameters. The black line represents the total error calculated as the root-sum-square values for the investigated spectroscopic parameters. The total error is around 4 % at pressures lower than 0.05 hPa. The largest contribution comes from the uncertainty in  $\gamma_{\text{air}}$  among those from spectroscopic parameters. The error due to 3 % uncertainty in  $\gamma_{\text{air}}$  is about 5 % for all pressures and the maximum is 27 pptv (8 %) at 1 hPa. We see that the sign of the VMR difference reverses at around 7 hPa. When the  $\gamma_{\text{air}}$  value is larger, the intensity around the line center of the synthesized spectrum is lower while the intensities in the wings are higher. The VMR at higher pressures is retrieved from the wings of the CIO lines, whereas that at lower pressures is derived from the line center. The rate of the contribution from the line center versus the contribution from the wings increases with altitude. Therefore, using a larger value of  $\gamma_{\text{air}}$ , a smaller VMR is retrieved at higher pressures and larger VMR is retrieved at lower pressures.

The error from  $n_{\text{air}}$  follows that from  $\gamma_{\text{air}}$ . The vertical trends of the errors from  $\gamma_{\text{air}}$  and  $n_{\text{air}}$  are similar. According to the definition of Eq. (3), increasing  $n_{\text{air}}$  increases  $\gamma_{\text{air}}$  in an atmosphere whose temperature is lower than 296 K. Such a temperature condition is satisfied at most altitudes observed by SMILES. The uncertainty in line intensity propagates to the error in the CIO VMR almost straightforwardly at pressures lower than 50 hPa, but with an opposite sign; i.e. +1 % uncertainty in line intensity results in about –1 % relative error. The error from dry-air continuum model increased to more than 10 % at pressures higher than 10 hPa. The continuum model affects the baseline correction in the retrieval particularly at higher pressures. The spectral line shape of CIO broadens as pressure increases, which makes the distinction between CIO and

[Title Page](#)

[Abstract](#)

[Introduction](#)

[Conclusions](#)

[References](#)

[Tables](#)

[Figures](#)

◀

▶

◀

▶

[Back](#)

[Close](#)

[Full Screen / Esc](#)

[Printer-friendly Version](#)

[Interactive Discussion](#)

baseline signals more difficult. The error due to the uncertainty in  $\gamma_{\text{air}}$  of the ozone line at 650.732 GHz is negligibly small.

### 3.2.2 Error due to uncertainty in the instrument function

#### Uncertainty in the instrument-related part of the forward model

5 Figure 6 shows the error budgets for the instrument functions in the forward model; i.e. antenna beam pattern, characteristics of SBS and AOS response function. The black line represents the total error calculated as the root-sum-square value of the errors from the three instrument functions. The total error is less than 4 % at pressures between 0.1 and 10 hPa. The dominant factor is the AOS response function at pressures lower than 0.3 hPa. The CIO retrieval at lower pressures is more sensitive to the 10 AOS response function since the spectral line width becomes comparable to or smaller than the width of the AOS response function.

15 The error from the ANT is the largest among the instrument functions between 0.6 and 10 hPa. We individually calculated the errors due to the 2 % uncertainty in the beam size and the lack of adjustment of antenna movement during data integration time for a spectrum at one tangent height. The error from ANT shown in Fig. 6 is the root-sum-square value of these errors. The error from SBS is the root-sum-square value of the errors due to the  $\pm 3$  dB uncertainty in  $\beta^{\text{USB}}$  and assuming  $\beta^{\text{USB}} = 1$  in the L2r retrieval processing. Comparing these three instruments, the error from SBS has 20 small contribution.

#### Uncertainty in the spectrum calibration

Figure 7 shows the error budgets due to the uncertainties in the calibration parameters; i.e. gain-compression parameter  $\alpha$ , main beam efficiency  $\eta_{\text{main}}$ , Joule loss of mirrors  $\mu$  and the temperature of the Earth  $T_{\text{earth}}$ . The total error is given by the root-sum-square of the errors due to the uncertainties in these calibration parameters and is about 1 %

[Title Page](#)

[Abstract](#)

[Introduction](#)

[Conclusions](#)

[References](#)

[Tables](#)

[Figures](#)

[◀](#)

[▶](#)

[◀](#)

[▶](#)

[Back](#)

[Close](#)

[Full Screen / Esc](#)

[Printer-friendly Version](#)

[Interactive Discussion](#)

between 0.01 and 20 hPa. The error from  $\alpha$  is the largest and followed by that from  $\eta_{\text{main}}$ . The error from  $\mu$  is given by the root-sum-square of the individually calculated errors in the 0.1 % uncertainties in Joule losses of MR, SR, TR and SWM. The errors from  $\mu$  and  $T_{\text{earth}}$  are negligible.

5 We calculated the effect from taking into account the nonlinearity between the AOS output  $V$  and brightness temperature  $\mathcal{T}$ , which is shown by the cyan line in Fig. 7 named “Non Lin.”. It has the contribution of as large as approximately 5 % relative error in the ClO retrieval, which is about five times larger than the total error from the uncertainty in calibration parameters. It clearly indicates that careful consideration of  
10 the nonlinearity between  $V$  and  $\mathcal{T}$  is essential for spectrum calibration.

### 3.2.3 Summary of the systematic error

Figure 8 shows  $E_{\text{systematic}}$  and its main components such as errors due to the uncertainties in  $\gamma_{\text{air}}$  and  $n_{\text{air}}$  of the ClO transition, the width of the AOS response function and  $\alpha$ .  $E_{\text{systematic}}$  is smaller than 10 pptv at all pressures except for around 1 hPa, where ClO  
15 concentrates. In the region of pressure higher than 0.1 hPa, uncertainties in  $\gamma_{\text{air}}$  and  $n_{\text{air}}$  are dominant. The error from the AOS response function is the largest followed by that from  $\gamma_{\text{air}}$  at lower pressures lower than 0.1 hPa. The gain-compression parameter ( $\alpha$ ) has the largest effect among the calibration parameters, but the error from  $\alpha$  is smaller than the other errors shown in Fig. 8.

20 There is a peak at about 2 hPa (40 km) in the VMR error. It may be because of the assumed ClO VMR profile; i.e. a priori profile  $x_a$  which has the VMR maximum at 40 km. The errors due to uncertainties in  $\gamma_{\text{air}}$  and  $n_{\text{air}}$ , large error sources in  $E_{\text{systematic}}$ , depend on the retrieved VMR value. The VMR value in  $x_a$  rapidly decrease at pressures lower than 2 hPa (40 km) and the peak of relative error locate at 1 hPa (45 km).

25 Totally, the error due to  $\gamma_{\text{air}}$  makes the largest contribution to  $E_{\text{systematic}}$ . The uncertainties in laboratory measurements of  $\gamma_{\text{air}}$  are difficult to reduce because of, for example, experimental systematic errors such as errors in the measurement of pressure and the difficulty of maintaining the stable temperature condition during measurement

[Title Page](#)[Abstract](#)[Introduction](#)[Conclusions](#)[References](#)[Tables](#)[Figures](#)[◀](#)[▶](#)[◀](#)[▶](#)[Back](#)[Close](#)[Full Screen / Esc](#)[Printer-friendly Version](#)[Interactive Discussion](#)

(Sato et al., 2010), and contamination with undesirable species (Oh and Cohen, 1994). Moreover, the theoretical prediction of  $\gamma_{\text{air}}$  has not been completely established. We conclude that the uncertainty in  $\gamma_{\text{air}}$  remains a large error source of the CIO retrieval.

### 3.3 Total error

5 Figure 9 shows  $E_{\text{random}}$ ,  $E_{\text{systematic}}$  and  $E_{\text{total}}$  for a single-scan observation and the averaging of  $N (= 100, 500)$  profiles. For a single-scan observation,  $E_{\text{random}}$  is larger than  $E_{\text{systematic}}$  and is dominant in  $E_{\text{total}}$  at all pressures. Averaging 100 profiles,  $E_{\text{random}}(100)$  is less than 10 pptv (10 %) at pressures higher than 0.2 hPa. In this region,  $E_{\text{systematic}}$  is dominant in  $E_{\text{total}}(100)$ . In the pressure region lower than 0.2 hPa,  $E_{\text{random}}(100)$  is still as large as 10–20 pptv. When 500 profiles are averaged,  $E_{\text{random}}(500)$  is less than 10 pptv (20 %) at all pressures.

10

We compare the errors in the CIO VMR observed by SMILES L2r (v2.1.5), UARS/MLS (v5), Aura/MLS (v3-3) and Odin/SMR (Chalmers v2.1) estimated by this work, Livesey et al. (2003), Livesey et al. (2011) and Urban et al. (2006), respectively.

15 The systematic errors, random errors ( $1 - \sigma$ ) for a single scan observation and vertical resolutions at 0.5, 2 and 10 hPa are summarized in Table 3. Systematic errors of SMILES, UARS/MLS and Aura/MLS are the same order of 10–50 pptv. Random errors of SMILES are about ten times smaller than those of the other instruments because of the low-noise spectra observed using the SIS mixers. The vertical resolution of SMILES is larger than those of Aura/MLS and Odin/SMR.

20

## 4 CIO diurnal variation

### 4.1 Evaluation of the SMILES CIO diurnal variation

Figure 10 shows the diurnal variations of SMILES CIO observations of zonal mean profiles for mid-latitude ( $40^{\circ}$  N– $50^{\circ}$  N) and equatorial ( $5^{\circ}$  S– $5^{\circ}$  N) regions at pressures of 10 hPa (30 km), 4.6 hPa (35 km), 2.1 hPa (41 km), 1 hPa (47 km), 0.46 hPa (53 km) and

[Title Page](#)

[Abstract](#)

[Introduction](#)

[Conclusions](#)

[References](#)

[Tables](#)

[Figures](#)

[◀](#)

[▶](#)

[◀](#)

[▶](#)

[Back](#)

[Close](#)

[Full Screen / Esc](#)

[Printer-friendly Version](#)

[Interactive Discussion](#)

## Error analysis and diurnal variation of SMILES CIO observation

T. O. Sato et al.

[Title Page](#)

[Abstract](#)

[Introduction](#)

[Conclusions](#)

[References](#)

[Tables](#)

[Figures](#)

◀

▶

◀

▶

[Back](#)

[Close](#)

[Full Screen / Esc](#)

[Printer-friendly Version](#)

[Interactive Discussion](#)

0.18 hPa (60 km). The two months data of SMILES were averaged during January–February in 2010. The criteria for the data selection are the measurement response  $>0.8$  (Eq. 19) and  $\chi^2 < 1$  (Eq. 13). The numbers of SMILES profiles averaged for each 1 h local time bin are 43–299 and 6–339 for the mid-latitude region ( $40^\circ$  N– $50^\circ$  N) and equatorial region ( $5^\circ$  S– $5^\circ$  N), respectively. The UARS/MLS observations (Ricaud et al., 2000) are presented in Fig. 10 to compare with the SMILES observations. The UARS/MLS CIO data for February at mid-latitude are averaged over seven years (from 1991 to 1997). Arbitrary offsets are added as 100, 200, 400, 200 and 100 pptv at 0.46, 1, 2.1, 4.6 and 10 hPa, respectively, for UARS/MLS CIO observation. Vertical error bars represent  $1 - \sigma$  standard deviations for both SMILES and UARS/MLS.

The night-time CIO VMR values near zero during 00:00–06:00 (a.m.) in the middle stratosphere such as at 10 hPa (about 30 km) and 4.6 hPa (35 km). In these time and pressure regions, the standard deviations represent the internal error in the SMILES CIO observation, not the natural variations. The standard deviations are about 20–30 pptv and consistent with the random error of 30 pptv estimated in this error analysis. It shows that the results in the error analysis are realistic.

The amplitudes of the observed CIO diurnal variations of 100–300 pptv are significantly larger than the random error of 30 pptv for 100 averaged profiles and the systematic error for SMILES of 10–30 pptv at all pressures. Moreover, there is good agreement between the behaviors of the diurnal variations in the CIO VMR for the stratosphere deduced from SMILES observations and UARS/MLS observations as shown in Fig. 3. We conclude that the CIO diurnal variations observed by SMILES are qualitatively reliable.

## 4.2 Global CIO diurnal variation

Global diurnal variations of CIO are shown in Fig. 11 as a function of the solar zenith angle (SZA) over the SMILES observation period from 12 October 2009 to 21 April 2010 in the stratosphere and mesosphere for the zonal means of  $40^\circ$  S– $20^\circ$  S,  $20^\circ$  S– $20^\circ$  N,  $20^\circ$  N– $50^\circ$  N and  $50^\circ$  S– $65^\circ$  N. The interval of color counter levels is representative of a VMR of 25 pptv, which is the total error value estimated in this study for averaging

## Error analysis and diurnal variation of SMILES CIO observation

T. O. Sato et al.

[Title Page](#)

[Abstract](#)

[Introduction](#)

[Conclusions](#)

[References](#)

[Tables](#)

[Figures](#)

[◀](#)

[▶](#)

[◀](#)

[▶](#)

[Back](#)

[Close](#)

[Full Screen / Esc](#)

[Printer-friendly Version](#)

[Interactive Discussion](#)

2009 and fade in March–April 2010. The amplitude of CIO enhancement is about 100 pptv, which is larger than the total error of 20–30 pptv at 70 km averaging 100 profiles.

## 5 Conclusions

SMILES observed strato- and mesospheric CIO at latitudes between 38° S–65° N. We quantitatively investigated the error in CIO L2r product version 2.1.5 including the errors due to spectrum noise, smoothing, uncertainties in the radiative transfer calculation and instrument functions and inaccuracy in the spectrum calibration. The total error for a single-scan observation is less than about 50 pptv at pressures between 0.1 and 60 hPa. The total error decreases to 10–30 pptv (about 10 %) at pressures between 0.01 hPa (about 80 km) and 100 hPa (about 16 km) with the averaging of 100–500 profiles. The largest effect on the systematic error is from the air-broadening coefficient,  $\gamma_{\text{air}}$ , which rises to 8 % in the total systematic error of 10 % at a pressure of 2 hPa (about 42 km).

We presented the global CIO diurnal variations in the stratosphere and mesosphere. The diurnal variation of stratospheric CIO is in good agreement with that of UARS/MLS. The behavior of the diurnal variation in CIO was reasonably explained by known diurnal chemistry. The global diurnal variation of CIO from the stratopause to the mesosphere were obtained for the first time by the SMILES observations. A night-time enhancement of CIO at a pressure of 0.02 hPa (about 70 km) was detected over the near polar region in January–February 2010. The quantitative error analysis shows that these CIO features are reliable.

**Acknowledgements.** JEM/SMILES mission is a joint project of the Japan Aerospace Exploration Agency (JAXA) and National Institute of Information and Communications Technology (NICT). The authors wish to acknowledge M. Shiotani (Kyoto University), M. Suzuki (ISAS/JAXA), and colleagues at JAXA and NICT for managing and supporting the SMILES mission. The authors thank K. Muranaga (Systems Engineering Consultants Co. Ltd.) and J. Möller

[Title Page](#)

[Abstract](#)

[Introduction](#)

[Conclusions](#)

[References](#)

[Tables](#)

[Figures](#)

[◀](#)

[▶](#)

[◀](#)

[▶](#)

[Back](#)

[Close](#)

[Full Screen / Esc](#)

[Printer-friendly Version](#)

[Interactive Discussion](#)

(Molflow Co. Ltd.) for supporting data processing of the Level-2 research product. The authors thank K. Suzuki for providing technical supports. The author TOS thanks H. Kanamori and N. Yoshida (Tokyo Institute of Technology) for their kind support. TOS is supported by a Grant in Aid for Research Fellowship for Young Scientists DC1 (No. 23-9766) from the Japan Society

5 for the Promotion of Science, and the Global COE program “Earth to Earths” of the Ministry of Education, Culture, Sports, and Technology, Japan. YK is supported by Funding Program for Next Generation World-Leading Researchers (NEXT Program) (No. GR101).

## References

Baron, P., Ricaud, P., de La Noë, J., Eriksson, J. E. P., Merino, F., Ridal, M., and Murtagh, D. P.:  
10 Studies for the Odin sub-millimetre radiometer, II. Retrieval methodology, *Can. J. Phys.*, 80, 341, doi:10.1139/p01-150, 2002. 4680

Baron, P., Mendrok, J., Kasai, Y., Ochiai, S., Seta, T., Sagi, K., Suzuki, K., Sagawa, H., and  
Urban, J.: AMATERAU: Model for atmospheric terahertz radiation analysis and simulation, *J. Natl. Inform. Commun. Technol.*, 55, 109–121, 2008. 4671

15 Baron, P., Urban, J., Sagawa, H., Möller, J., Murtagh, D. P., Mendrok, J., Dupuy, E., Sato, T. O.,  
Ochiai, S., Suzuki, K., Manabe, T., Nishibori, T., Kikuchi, K., Sato, R., Takayanagi, M., Mu-  
rayama, Y., Shiotani, M., and Kasai, Y.: The Level 2 research product algorithms for the Su-  
perconducting Submillimeter-Wave Limb-Emission Sounder (SMILES), *Atmos. Meas. Tech.*,  
4, 2105–2124, doi:10.5194/amt-4-2105-2011, 2011. 4671, 4672, 4678

20 Boissoles, J., Boulet, C., Tipping, R. H., Brown, A., and Ma, Q.: Theoretical calculation  
of the translation-rotation collision-induced absorption in  $N_2$ - $N_2$ ,  $O_2$ - $O_2$ , and  $N_2$ - $O_2$  pairs,  
*J. Quant. Spectrosc. Ra.*, 82, 505–516, doi:10.1016/S0022-4073(03)00174-2, 2003. 4672

Cazzoli, G. and Puzzarini, C.: Hyperfine structure of the  $J = 1 \leftarrow 0$  transition of  $H^{35}Cl$  and  $H^{37}Cl$ :  
improved ground state parameters, *J. Mol. Spectrosc.*, 226, 161–168, 2004. 4672

25 Drouin, B. J.: Submillimeter measurements of  $N_2$  and air broadening of hypochlorous acid,  
*J. Quant. Spectrosc. Ra.*, 103, 558–564, doi:10.1016/j.jqsrt.2006.07.007, 2007. 4672

Drouin, B. J. and Gamache, R. R.: Temperature dependent air-broadened linewidths of ozone  
rotational transitions, *J. Mol. Spectrosc.*, 251, 194–202, doi:10.1016/j.jms.2008.02.016,  
2008. 4672, 4673

[Title Page](#)

[Abstract](#)

[Introduction](#)

[Conclusions](#)

[References](#)

[Tables](#)

[Figures](#)

◀

▶

[Back](#)

[Close](#)

[Full Screen / Esc](#)

[Printer-friendly Version](#)

[Interactive Discussion](#)

**Error analysis and diurnal variation of SMILES CIO observation**

T. O. Sato et al.

[Title Page](#)[Abstract](#)[Introduction](#)[Conclusions](#)[References](#)[Tables](#)[Figures](#)[◀](#)[▶](#)[◀](#)[▶](#)[Back](#)[Close](#)[Full Screen / Esc](#)[Printer-friendly Version](#)[Interactive Discussion](#)

Markov, V. N. and Krupnov, A. F.: Measurements of the pressure shift of the  $1_{10}-1_{01}$  water line at 556 GHz produced by mixtures of gases, *J. Mol. Spectrosc.*, 172, 211–214, 1995. 4672

Masuko, H., Shiotani, M., and SMILES mission team: JEM/SMILES Mission Plan, version 2.1., Tech. Rep. NASDA/CRL, National Space Development Agency of Japan, and Communications Research Laboratory, available at: [http://smiles.nict.go.jp/Mission\\_Plan](http://smiles.nict.go.jp/Mission_Plan) (last access: 29 June 2012), 2002. 4673

Mizobuchi, S., Kikuchi, K., Ochiai, S., Nishibori, T., Sano, T., Tamaki, K., and Ozeki, H.: In-orbit measurement of the AOS (Acousto-Optical Spectrometer) response using frequency comb signals, *IEEE J. Sel. Topics Appl. Earth Obs. Remote Sens.*, 5, 977–983 2012. 4675

Mizoguchi, A., Yagi, T., Kondo, K., Sato, T. O., and Kanamori, H.: Submillimeter-wave measurements of  $N_2$  and  $O_2$  pressure broadening for  $HO_2$  radical generated by Hg-photosensitized reaction, *J. Quant. Spectrosc. Ra.*, 113, 279–285, doi:10.1016/j.jqsrt.2011.11.009, 2012. 4672

Murtagh, D., Frisk, U., Merino, F., Ridal, M., Jonsson, A., Stegman, J., Witt, G., Eriksson, P., Jiménez, C., Megie, G., de La Noë, J., Ricaud, P., Baron, P., Pardo, J. R., Hauchcorne, A., Llewellyn, E. J., Degenstein, D. A., Gattiner, R. L., Lloyd, N. D., Evans, W. F. J., McDade, I. C., Haley, C. S., Sioris, C., von Savigny, C., Solheim, B. H., McConnell, J. C., Strong, K., Richardson, E. H., Leppelmeier, G. W., Kyrölä, E., Auvinen, H., and Oikarinen, L.: An overview of the Odin atmospheric mission, *Can. J. Phys.*, 80, 309–318, doi:10.1139/p01-157, 2002. 4669

Ochiai, S., Nishibori, T., Ozeki, H., Kikuchi, K., and Manabe, T.: Superconducting submillimeter-wave limb-emission sounder on the international space station I: radiometric and spectral calibration and data processing, *J. Natl. Inform. Commun. Technol.*, 55, 83–95, 2008. 4675, 4678

Ochiai, S., Kikuchi, K., Nishibori, T., and Manabe, T.: Gain nonlinearity calibration of submillimeter radiometer for JEM/SMILES, *J. Sel. Topics Appl. Earth Obs. Remote Sens.*, 5, 962–969, 2012a. 4677

Ochiai, S., Kikuchi, K., Nishibori, T., Manabe, T., Ozeki, H., Mizobuchi, S., and Irimajiri, Y.: Receiver performance of Superconducting Submillimeter-Wave Limb-Emission Sounder (SMILES) on the International Space Station, *IEEE T. Geosci. Remote*, submitted, 2012b. 4673

## Error analysis and diurnal variation of SMILES CIO observation

T. O. Sato et al.

[Title Page](#)

[Abstract](#)

[Introduction](#)

[Conclusions](#)

[References](#)

[Tables](#)

[Figures](#)

[◀](#)

[▶](#)

[Back](#)

[Close](#)

[Full Screen / Esc](#)

[Printer-friendly Version](#)

[Interactive Discussion](#)

Oh, J. and Cohen, E. A.: Pressure broadening of ClO by N<sub>2</sub> and O<sub>2</sub> near 204 and 649 GHz and new frequency measurements between 632 and 725 GHz, *J. Quant. Spectrosc. Ra.*, 52, 151–156, doi:10.1016/0022-4073(94)90004-3, 1994. 4672, 4687

5 Pardo, J. R., Serabyn, E., and Cernicharo, J.: Submillimeter atmospheric transmission measurements on Mauna Kea during extremely dry El Niño conditions: implications for bread-band opacity contributions, *J. Quant. Spectrosc. Ra.*, 68, 419–433, 2001. 4672

Perrin, A., Puzzarini, C., Colmont, J. M., Verdes, C., Wlodarczak, G., Cazzoli, G., Buehler, S., Flaud, J. M., and Demaison, J.: Molecular line parameters for the “MASTER” (millimeter wave acquisitions for stratosphere/troposphere exchange research) database, *J. Atmos. Chem.*, 51, 161–205, 2005. 4672

10 Pickett, H. M., Poynter, R. L., Cohen, E. A., Delitsky, M. L., Pearson, J. C., and Müller, H. S. P.: Submillimeter, millimeter and microwave spectral line catalog., *J. Quant. Spectrosc. Ra.*, 60, 883–890, doi:10.1016/S0022-4073(98)00091-0, 1998. 4672, 4697

15 Ricaud, P., Chipperfield, M. P., Waters, J. W., Russell III, J. M., and Roche, A. E.: Temporal evolution of chlorine monoxide in the middle stratosphere, *J. Geophys. Res.*, 105, 4459–4470, doi:10.1029/1999JD900995, 2000. 4688, 4709

20 Riener, M. M., Suarez, M. J., Todling, R., Bacmeister, J., Takacs, L., Liu, H.-C., Gu, W., Sienkiewicz, M., Koster, R. D., Gelaro, R., Stajner, I., and Nielsen, J. E.: The GEOS-5 Data Assimilation System – Documentation of Versions 5.0.1, 5.1.0, and 5.2.0., *Tech. Rep. NASA/TM-2008-104606*, vol. 27, National Aeronautics and Space Administration, available online: <http://mls.jpl.nasa.gov/data/datadocs.php> (last access: 29 June 2012), 2008. 4673

Rodgers, C. D.: *Inverse Methods for Atmospheric Sounding: Theory and Practice*, Series on Atmospheric, Oceanic and Planetary Physics, vol. 2, World Scientific, Singapore, 3605–3609, 2000. 4678

25 Rothman, L. S., Gordon, I. E., Barbe, A., Benner, D. C., Bernath, P. F., Birk, M., Boudon, V., Brown, L. R., Campargue, A., Champion, J.-P., Chance, K., Coudert, L. H., Dana, V., Devi, V. M., Fally, S., Flaud, J.-M., Gamache, R. R., Goldman, A., Jacquemart, D., Kleiner, I., Lacome, N., Lafferty, W. J., Mandin, J.-Y., Massie, S. T., Mikhailenko, S. N., Miller, C. E., Moazzen-Ahmadi, N., Naumenko, O. V., Nikitin, A. V., Orphal, J., Perevalov, V. I., Perrin, A., Predoi-Cross, A., Rinsland, C. P., Rotger, M., Šimečková, M., Smith, M. A. H., Sung, K., Tashkun, S. A., Tennyson, J., Toth, R. A., Vandaele, A. C., and Vander Auwera, J.: The HITRAN 2008 molecular spectroscopic database, *J. Quant. Spectrosc. Ra.*, 110, 533–572, doi:10.1016/j.jqsrt.2009.02.013, 2009. 4672

Title Page

Abstract Introduction

Conclusions References

Tables Figures

◀

▶

◀

▶

Back

Close

Full Screen / Esc

Printer-friendly Version

Interactive Discussion

**Error analysis and diurnal variation of SMILES CIO observation**

T. O. Sato et al.

[Title Page](#)[Abstract](#)[Introduction](#)[Conclusions](#)[References](#)[Tables](#)[Figures](#)[◀](#)[▶](#)[◀](#)[▶](#)[Back](#)[Close](#)[Full Screen / Esc](#)[Printer-friendly Version](#)[Interactive Discussion](#)

Waters, J. W., Froidevaux, L., Harwood, R. S., Jarnot, R. F., Pickett, H. M., Read, W. G., Siegel, P. H., Cofield, R. E., Filipiak, M. J., Flower, D. A., Holden, J. R., Lau, G. K., Livesey, N. J., Manney, G. L., Pumphrey, H. C., Santee, M. L., Wu, D. L., Cuddy, D. T., Lay, R. R., Loo, M. S., Perun, V. S., Schwartz, M. J., Stek, P. C., Thurstans, R. P., Boyles, M. A., Chandra, K. M., Chavez, M. C., Chen, G.-S., Chudasama, B. V., Dodge, R., Fuller, R. A., Giard, M. A., Jiang, J. H., Jiang, Y., Knosp, B. W., Labelle, R. C., Lam, J. C., Lee, A. K., Miller, D., Oswald, J. E., Patel, N. C., Pukala, D. M., Quintero, O., Scaff, D. M., Vansnyder, W., Tope, M. C., Wagner, P. A., and Walch, M. J.: The Earth Observing System Microwave Limb Sounder (EOS MLS) on the aura satellite, *IEEE T. Geosci. Remote*, 44, 1075–1092, doi:10.1109/TGRS.2006.873771, 2006. 4669

5

10

Discussion Paper | Discussion Paper

## Error analysis and diurnal variation of SMILES CIO observation

T. O. Sato et al.

[Title Page](#)[Abstract](#)[Introduction](#)[Conclusions](#)[References](#)[Tables](#)[Figures](#)[◀](#)[▶](#)[◀](#)[▶](#)[Back](#)[Close](#)[Full Screen / Esc](#)[Printer-friendly Version](#)[Interactive Discussion](#)

## Error analysis and diurnal variation of SMILES CIO observation

T. O. Sato et al.

**Table 1.** Spectroscopic parameters of the CIO lines observed by SMILES. The number in parentheses represents the uncertainty. Intensity is represented by a base-10 logarithm. The quantum numbers are represented by  $J$ ,  $\Omega$ ,  $\Sigma$ ,  $\Lambda$  and  $F$  for the total angular momentum, projection of  $J$  on the molecular axis (z-axis), projection of total electron spin momentum on the z-axis, projection of total orbit momentum on the z-axis and real total angular momentum including nuclear spin momentum  $I = 3/2$  ( $\Omega = \Sigma + \Lambda$ ,  $F = J + I$ ).

Frequency <sup>a</sup> (GHz)	Intensity <sup>a</sup> (MHz nm <sup>2</sup> )	$\gamma_{\text{air}}^{\text{b}}$ (MHz Torr <sup>-1</sup> )	$n_{\text{air}}^{\text{b}}$ (–)	Quantum numbers (upper state) <sup>a</sup>						Quantum numbers (lower state) <sup>a</sup>								
				$J'$	$\Omega'$	$\Sigma'$	$\Lambda'$	$F'$	$J''$	$\Omega''$	$\Sigma''$	$\Lambda''$	$F''$	$J'$	$\Omega'$	$\Sigma'$	$\Lambda'$	$F'$
649.44504	–1.9671 (<1%)	2.86 (3%)	0.77 (10%)	35/2	3/2	1/2	–1	19	33/2	3/2	1/2	+1	18					
649.44504	–1.9920 (<1%)	2.86 (3%)	0.77 (10%)	35/2	3/2	1/2	–1	18	33/2	3/2	1/2	+1	17					
649.44504	–2.0170 (<1%)	2.86 (3%)	0.77 (10%)	35/2	3/2	1/2	–1	17	33/2	3/2	1/2	+1	16					
649.44504	–2.0420 (<1%)	2.86 (3%)	0.77 (10%)	35/2	3/2	1/2	–1	16	33/2	3/2	1/2	+1	15					
649.45117	–1.9671 (<1%)	2.86 (3%)	0.77 (10%)	35/2	3/2	1/2	+1	19	33/2	3/2	1/2	–1	18					
649.45117	–1.9920 (<1%)	2.86 (3%)	0.77 (10%)	35/2	3/2	1/2	+1	18	33/2	3/2	1/2	–1	17					
649.45117	–2.0170 (<1%)	2.86 (3%)	0.77 (10%)	35/2	3/2	1/2	+1	17	33/2	3/2	1/2	–1	16					
649.45117	–2.0420 (<1%)	2.86 (3%)	0.77 (10%)	35/2	3/2	1/2	+1	16	33/2	3/2	1/2	–1	15					

<sup>a</sup> The JPL catalog version 3 Pickett et al. (1998).

<sup>b</sup> W. G. Read, personal communication, 2011.

[Title Page](#)

[Abstract](#)

[Introduction](#)

[Conclusions](#)

[References](#)

[Tables](#)

[Figures](#)

[◀](#)

[▶](#)

[◀](#)

[▶](#)

[Back](#)

[Close](#)

[Full Screen / Esc](#)

[Printer-friendly Version](#)

[Interactive Discussion](#)

## Error analysis and diurnal variation of SMILES CIO observation

T. O. Sato et al.

[Title Page](#)

[Abstract](#)

[Introduction](#)

[Conclusions](#)

[References](#)

[Tables](#)

[Figures](#)

◀

▶

◀

▶

[Back](#)

[Close](#)

[Full Screen / Esc](#)

[Printer-friendly Version](#)

[Interactive Discussion](#)

**Table 2.** Summary of error sources for a single-scan observation.

Systematic (S) or Random (R)	Error source	Uncertainty in error source	Error at 2.5 hPa (pptv)	Calculation method
R	Spectrum noise	$\epsilon_y^1$	14	Eq. (23)
R	Smoothing error	$\epsilon_a^2$	2.9	Eq. (24)
R	Temperature profile	footnote <sup>3</sup>	9.2	Eq. (25)
R	Pressure profile	10 %	20	Eq. (25)
S	Line intensity <sup>4</sup>	1 %	6.3	Eq. (25)
S	$\gamma_{\text{air}}$ (Air-broadening coefficient) <sup>4</sup>	3 %	17	Eq. (25)
S	$n_{\text{air}}$ (Temperature dependence of $\gamma_{\text{air}}$ ) <sup>4</sup>	10 %	15	Eq. (25)
S	$\gamma_{\text{air}}$ of the O <sub>3</sub> line at 650.732 GHz	3 %	0.022	Eq. (25)
S	Dry-air continuum	20 %	3.5	Eq. (25)
S	Antenna beam pattern	footnote <sup>5</sup>	3.8	Eq. (25)
S	SBS characteristics	footnote <sup>6</sup>	0.13	Eq. (25)
S	AOS response function	10 % in FWHM	0.24	Eq. (25)
S	Gain-compression parameter $\alpha$	20 %	6.2	Eq. (31)
S	Main beam efficiency $\eta_{\text{main}}$	2 %	1.9	Eq. (31)
S	Joule loss of mirrors $\mu$	0.1 %	0.042	Eq. (31)
S	Temperature of earth $T_{\text{earth}}$	20 K	0.010	Eq. (31)

<sup>1</sup> Given by Eq. (14).

<sup>2</sup> Given by Eq. (16).

<sup>3</sup> 3 K in the troposphere, 10 K in the stratosphere, 30 K in the mesosphere and 50 K in the thermosphere.

<sup>4</sup> Of the CIO lines at 649.445 and 649.451 GHz.

<sup>5</sup> 2 % uncertainty in FWHM of  $R^{\text{ANT}}$  and no adjustment of six steps in one tangent height.

<sup>6</sup> Assuming  $\beta^{\text{USB}} = 1$  and  $\pm 3 \text{ dB}$  in  $\beta^{\text{USB}}$ .

## Error analysis and diurnal variation of SMILES CIO observation

T. O. Sato et al.

**Table 3.** Summary of errors ( $1 - \sigma$ ) for a single-scan observation of CIO products observed by SMILES, UARS/MLS, Aura/MLS and Odin/SMR. Systematic error (SE), random error (RE) and vertical resolution (VR) for these instruments are listed.

Pressure (Altitude)	SMILES L2r (v2.1.5) <sup>1</sup>			UARS/MLS (v5) <sup>2</sup>			Aura/MLS (v3-3) <sup>3</sup>			Odin/SMR (Chalmers v2.1) <sup>4</sup>		
	SE (pptv)	RE (pptv)	VR (km)	SE (pptv)	RE (pptv)	VR (km)	SE (pptv)	RE (pptv)	VR (km)	SE (pptv)	RE (pptv)	VR (km)
0.5 hPa (50 km)	10	30	5.5	—	—	—	—	—	—	$\leq 100$	$\leq 150$	2.5–3
2 hPa (40 km)	30	40	4	50	400	6	25	100	3.5–4.5	$\leq 100$	$\leq 150$	2.5–3
10 hPa (30 km)	10	30	4	25	400	4	25	100	3.5–4.5	$\leq 100$	$\leq 150$	2.5–3

<sup>1</sup> This work.

<sup>2</sup> See Table 9 in Livesey et al. (2003).

<sup>3</sup> See Table 3.5.1 in Livesey et al. (2011).

<sup>4</sup> See Table 1 in Urban et al. (2006).

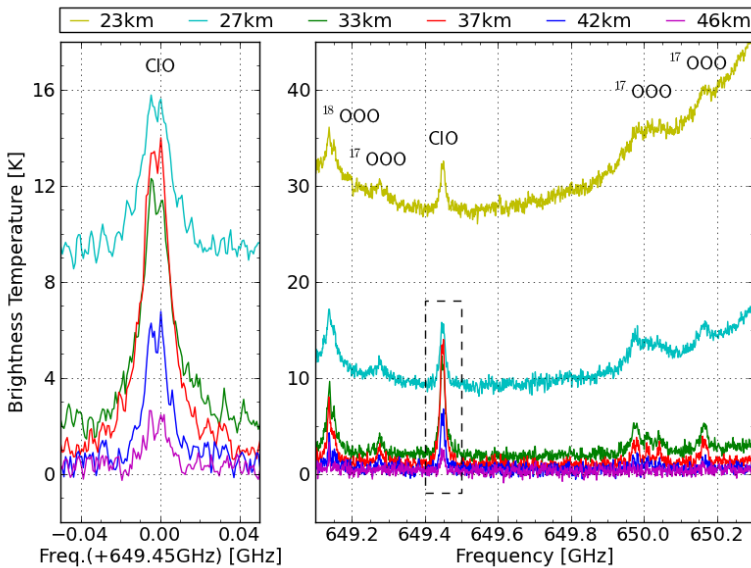


**Fig. 1.** Band C spectrum observed by SMILES at tangent heights of 23, 27, 33, 37, 42 and 46 km. The frequency is calibrated considering Doppler shift. The left figure is a magnification of the CIO transitions at 649.445 and 649.451 GHz. The right figure shows the full frequency region for band C. Date: 9 November 2009. Local time: 00:22. Latitude: 57.2° N. Longitude: 6.4° E.

Title Page	
Abstract	Introduction
Inclusions	References
Tables	Figures
◀	▶
◀	▶
Back	Close
Full Screen / Esc	

[Printer-friendly Version](#)

## Interactive Discussion

## Error analysis and diurnal variation of SMILES CIO observation

T. O. Sato et al.

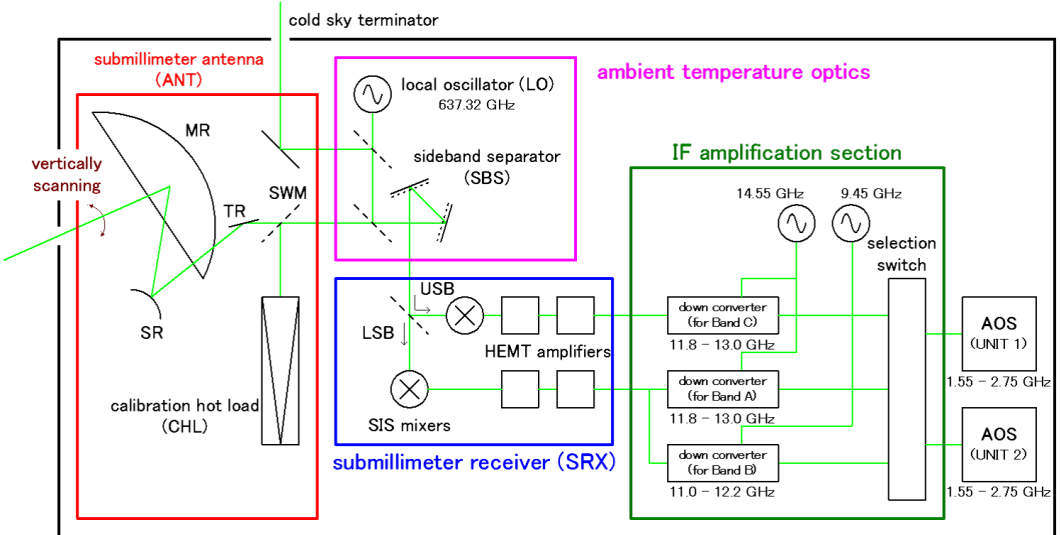


**Fig. 2.** Schematic diagram of the SMILES payload.

## Title Page

## Abstract

## Introduction

## Conclusion

## References

## Tables

## Figures

1

1

Back

Close

Full Screen / Esc

ANSWER

## Interactive Discussion

## Error analysis and diurnal variation of SMILES CIO observation

T. O. Sato et al.

## Title Page

## Abstract

Figures

A set of four blue navigation icons. From top-left to bottom-right: a left arrow, a right arrow, a left arrow, and a right arrow. Below the top row are the labels 'Back' and 'Close'.

Full Screen / Esc

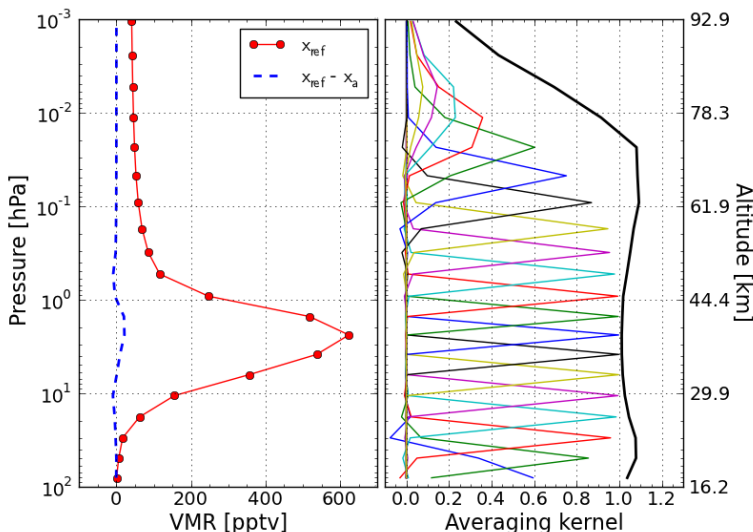


**Fig. 3.** The reference profile,  $x_{\text{ref}}$ , of the CIO VMR used in the error analysis. The left figure shows  $x_{\text{ref}}$  and the difference in  $x_a$  and  $x_{\text{ref}}$ . The right figure shows the measurement response (black solid line) and averaging kernels.

## Error analysis and diurnal variation of SMILES CIO observation

T. O. Sato et al.

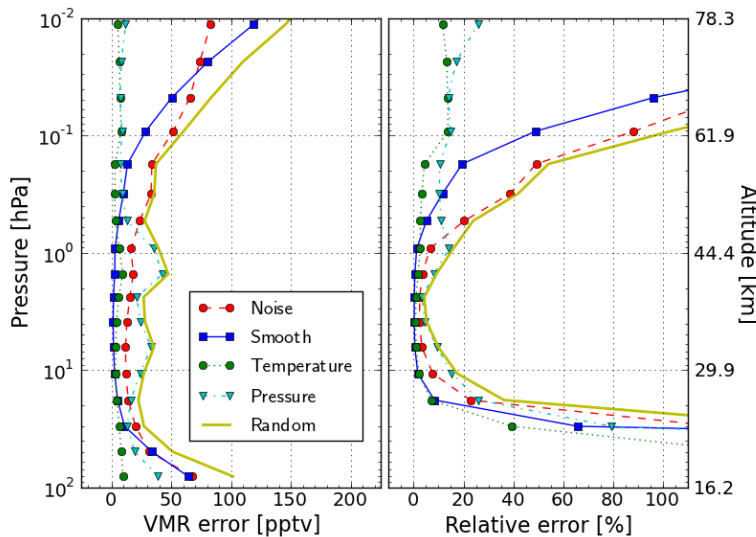


**Fig. 4.** Summary of random errors for a single-scan observation. (red)  $E_{\text{noise}}$ . (blue)  $E_{\text{smooth}}$ . (green) Error from the temperature profile; 3, 10, 30 and 50 K for the troposphere (below 11 km), the stratosphere (11–59 km), the mesosphere (59–96 km) and the thermosphere (above 96 km). (cyan) Error from the pressure profile (10 %). (yellow) Total random error.

- [Title Page](#)
- [Abstract](#) [Introduction](#)
- [Conclusions](#) [References](#)
- [Tables](#) [Figures](#)
- [◀](#) [▶](#)
- [◀](#) [▶](#)
- [Back](#) [Close](#)
- [Full Screen / Esc](#)

[Printer-friendly Version](#)

[Interactive Discussion](#)

## Error analysis and diurnal variation of SMILES CIO observation

T. O. Sato et al.

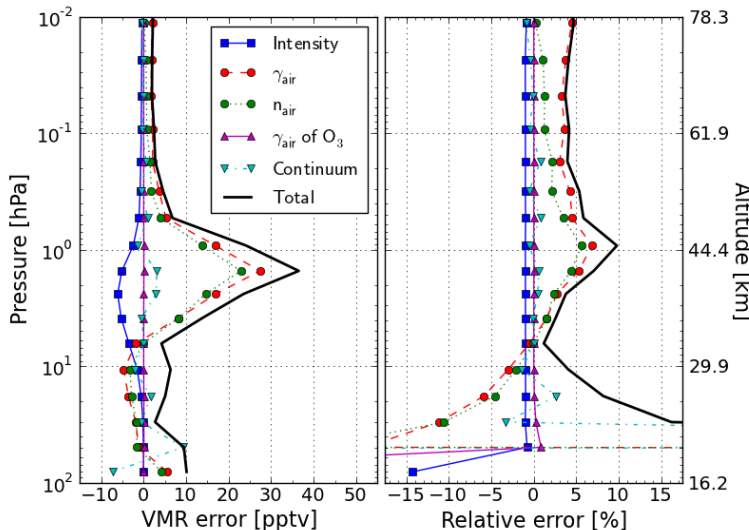


**Fig. 5.** Same as Fig. 4 but for the errors from spectroscopic parameters. (blue) +1% uncertainty in line intensity, (red) +3% uncertainty in  $\gamma_{\text{air}}$  and (green) +10% uncertainty in  $n_{\text{air}}$  of the CIO transitions at 649.445 and 649.451 GHz. (purple) +3% uncertainty in  $\gamma_{\text{air}}$  for the  $\text{O}_3$  transition at 650.732 GHz. (cyan) +20% uncertainty in the dry-air continuum. (black) Total error for the five components.

- [Title Page](#)
- [Abstract](#) [Introduction](#)
- [Conclusions](#) [References](#)
- [Tables](#) [Figures](#)
- [◀](#) [▶](#)
- [◀](#) [▶](#)
- [Back](#) [Close](#)
- [Full Screen / Esc](#)

[Printer-friendly Version](#)

[Interactive Discussion](#)

## Error analysis and diurnal variation of SMILES CIO observation

T. O. Sato et al.

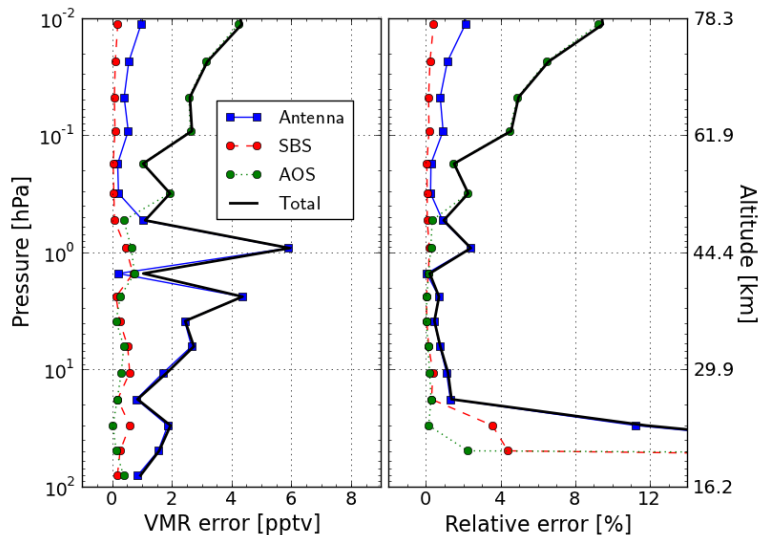


**Fig. 6.** Same as Fig. 4 but for the errors from instrument functions in the forward model. (blue) Error from the antenna beam pattern. (red) Error from the SBS. (green) 10% uncertainty in the width of the AOS response function. (black) Total error of the three components.

## Title Page

## Abstract

## Introduction

## Conclusion

## References

## Tables

## Figures

18



1

1

Full Screen / Esc

## Interactive Discussion

## Error analysis and diurnal variation of SMILES CIO observation

T. O. Sato et al.

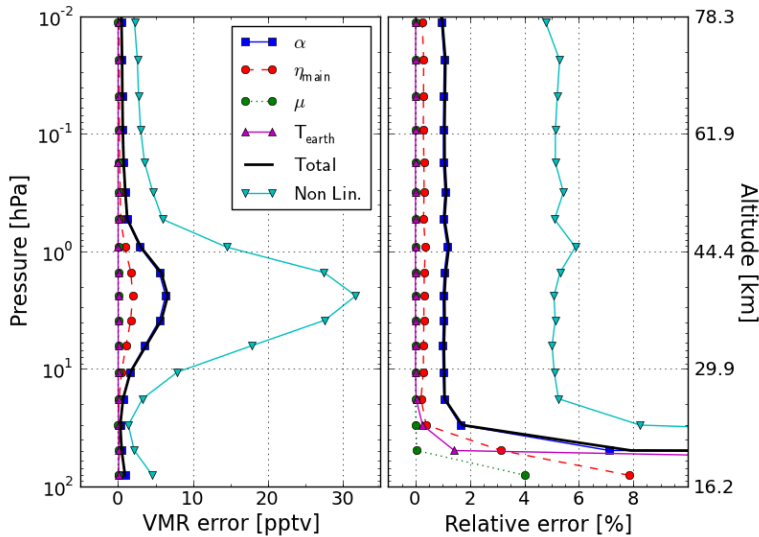


**Fig. 7.** Same as Fig. 4 but for the uncertainty in the calibration parameters. (blue) 20 % uncertainty in the gain-compression parameter  $\alpha$ . (red) 2 % uncertainty in the main beam efficiency  $\eta_{\text{main}}$ . (green) Total error due to 0.1 % uncertainties in Joule losses  $\mu$  for the mirrors (MR, SR, TR and SWM). (purple) 20 K uncertainty in the temperature of the Earth  $T_{\text{earth}}$ . (black) Total error due to the inaccuracy of the spectrum calibration. (cyan) The error due to neglecting the non linearity between brightness temperature  $\mathcal{T}$  and the AOS output  $V$ .

- [Title Page](#)
- [Abstract](#) [Introduction](#)
- [Conclusions](#) [References](#)
- [Tables](#) [Figures](#)
- [◀](#) [▶](#)
- [◀](#) [▶](#)
- [Back](#) [Close](#)
- [Full Screen / Esc](#)

[Printer-friendly Version](#)

[Interactive Discussion](#)

## Error analysis and diurnal variation of SMILES CIO observation

T. O. Sato et al.

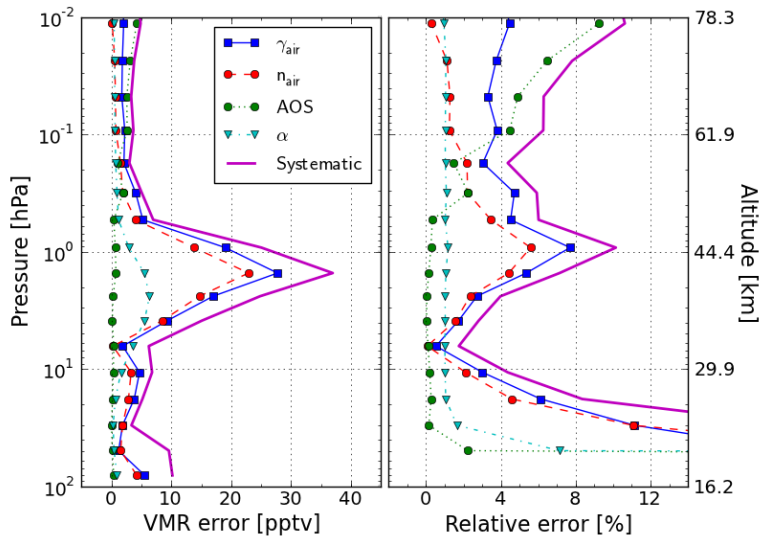


**Fig. 8.** Same as Fig. 4 but for the systematic error. The total systematic error and the errors from the main error sources are shown. (blue) 3 % uncertainty in  $\gamma_{\text{air}}$ . (red) 10 % uncertainty in  $n_{\text{air}}$ . (green) 10 % uncertainty in the width of the AOS response function. (cyan) 20 % uncertainty in  $\alpha$ . (purple) Total systematic error.

- [Title Page](#)
- [Abstract](#) [Introduction](#)
- [Conclusions](#) [References](#)
- [Tables](#) [Figures](#)
- [◀](#) [▶](#)
- [◀](#) [▶](#)
- [Back](#) [Close](#)
- [Full Screen / Esc](#)

- [Printer-friendly Version](#)
- [Interactive Discussion](#)

## Error analysis and diurnal variation of SMILES CIO observation

T. O. Sato et al.

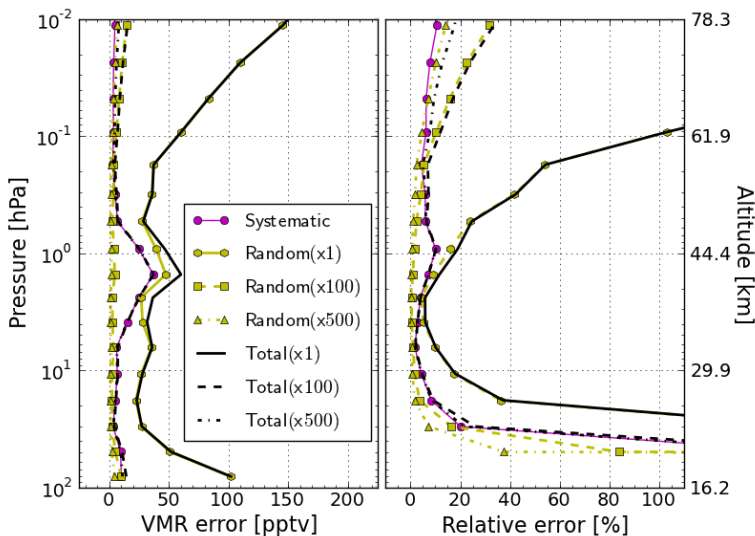


**Fig. 9.** Same as Fig. 4 but for the total error. Total error in the CIO retrieval for an averaging of  $N$  profiles ( $N = 1, 100$  and  $500$ ). (purple) Systematic error. (yellow) Random error when averaging  $N$  profiles. (black) Total error when averaging  $N$  profiles.

## Title Page

## Abstract

## Introduction

## Conclusion

## References

## Tables

## Figures

1

A small white triangle pointing right, indicating the next slide in a presentation.

◀



Back

Close

Full Screen / Esc

## Interactive Discussion

## Error analysis and diurnal variation of SMILES CIO observation

T. O. Sato et al.

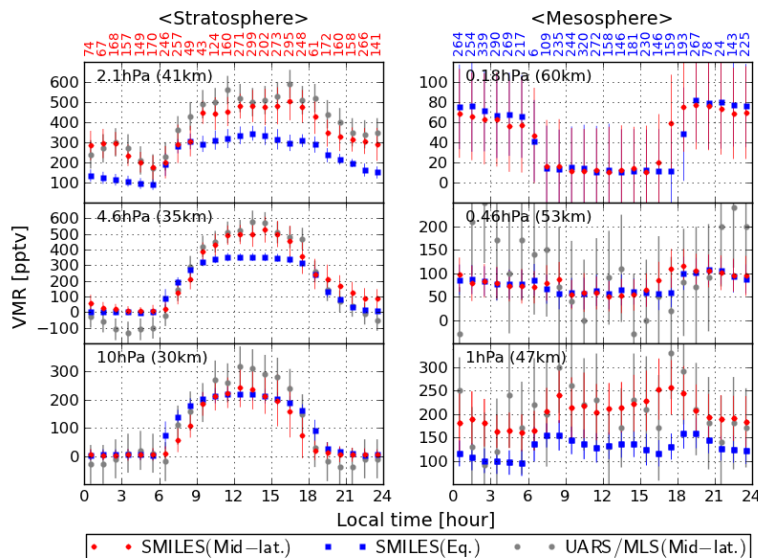


**Fig. 10.** CIO diurnal variations observed by SMILES and by UARS/MLS at the pressures 0.18, 0.46, 1, 2.1, 4.6 and 10 hPa for the zonal mean of  $40^{\circ}$  N– $50^{\circ}$  N and  $5^{\circ}$  S– $5^{\circ}$  N. (red) SMILES at  $40^{\circ}$  N– $50^{\circ}$  N. (blue) SMILES at  $5^{\circ}$  S– $5^{\circ}$  N. (gray) UARS/MLS at  $40^{\circ}$  N– $50^{\circ}$  N. The data are averaged within a local time bin of 1 h interval. Vertical error bars represent  $1 - \sigma$  standard deviations of the observation data. The numbers of profiles averaged at each local time for SMILES observations at  $40^{\circ}$  N– $50^{\circ}$  N and  $5^{\circ}$  S– $5^{\circ}$  N are indicated at the top of the left and right panels, respectively. The vertical grids for SMILES are adjusted to the UARS/MLS grids with linear interpolation. The SMILES data are taken for the observation period from January to February 2010, while UARS/MLS data are taken by averaging February data for the seven years from 1991 to 1997. The UARS/MLS data are taken from Fig. 1 in Ricaud et al. (2000). We add arbitrary offsets of 100, 200, 400, 200 and 100 pptv at 0.46, 1, 2.1, 4.6 and 10 hPa, respectively, since UARS/MLS data have a negative bias.

## Error analysis and diurnal variation of SMILES CIO observation

T. O. Sato et al.

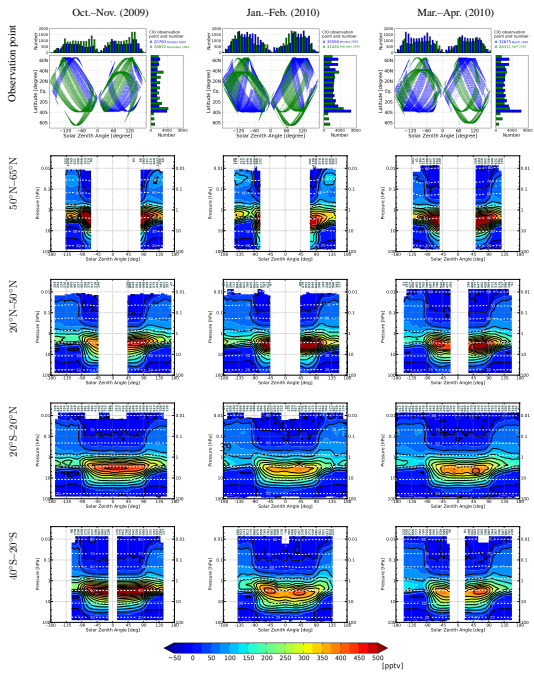


**Fig. 11.** Seasonal and latitudinal variations in CIO diurnal variations as a function of SZA and pressure for October–November 2009, January–February 2010 and March–April 2010 and latitudes ( $50^{\circ}$  N– $65^{\circ}$  N,  $20^{\circ}$  N– $50^{\circ}$  N,  $20^{\circ}$  S– $20^{\circ}$  N and  $40^{\circ}$  S– $20^{\circ}$  S). The color counter level is representative of a VMR of 25 pptv. The altitude is represented by a white dotted line. The number of averaged profiles in an SZA bin of  $10^{\circ}$  is shown in the top of each panel. Only the retrieved VMR that satisfies  $\chi^2 < 1$  and  $m > 0.8$  are used. In the top row, observation points are represented by dots of different color for each month. The numbers of scans in a SZA bin of  $10^{\circ}$  and a latitude bin of  $10^{\circ}$  are represented by bars above and to the right. Total scan number is given at in the upper right. Only the observation points that satisfy  $\chi^2 < 1$  are plotted.

## Title Page

## Abstract

## Introduction

## Conclusions

## References

## Tables

## Figures

1

A small blue triangle icon with a white outline, positioned in the bottom right corner of the slide.

Ba

Close

Full Screen / Esc

ANSWER

## Interactive Discussion